Am J Cancer Res 2026;16(8):3620-3643
www.ajcr.us /ISSN:2156-6976/ajcr0170877

Original Article

AI-assisted design and virtual profiling of targeted degraders for pancreatic cancer therapy via PROTAC technology

Bing Du[1*], Kunjie Wang[2*], Zhu Wu[3], Shaofan Qiu[4], Filippiadis Dimitrios Konstantinos[5], Shuo Yu[6]

[1]Department of Oncology, The Second Hospital of Hebei Medical University, Shijiazhuang 050000, Hebei, China; [2]Department of Oncology, Affiliated Hospital of Hebei University, Baoding 071000, Hebei, China; [3]The Hunan Provincial Key Laboratory of The TCM Agricultural Biogenomics, Changsha Medical University, Changsha 410219, Hunan, China; [4]Department of Gastrointestinal Surgery, The Second Hospital of Hebei Medical University, Shijiazhuang 050000, Hebei, China; [5]Evgenidion University Hospital, Athens 11528, Greece; [6]Department of Surgical Oncology, The Second Hospital of Hebei Medical University, Shijiazhuang 050000, Hebei, China. [*]Equal contributors.

Received December 19, 2025; Accepted June 27, 2026; Epub August 15, 2026; Published August 30, 2026

Abstract: Pancreatic cancer remains one of the most lethal malignancies because of late diagnosis, aggressive progression, therapy resistance, and limited effective treatment options. Bromodomain-containing protein 4 (BRD4) is an important epigenetic regulator implicated in pancreatic cancer progression through its role in transcriptional control, cell proliferation, and survival signaling. Targeted protein degradation using proteolysis-targeting chimeras (PROTACs) offers a potential strategy for eliminating disease-associated proteins through ubiquitin-proteasome-mediated degradation rather than transient pharmacological inhibition. In this study, an AI-assisted and structure-guided computational workflow was used to design and virtually prioritize BRD4-targeting PROTAC candidates recruiting DCAF15 as the E3 ligase component. The workflow integrated protein-structure evaluation, pharmacophore-based ligand screening, ADMET and Lipinski filtering, binary protein-ligand docking, molecular-interaction analysis, rational linker selection, BRD4-DCAF15 protein-protein docking, PROTAC-mediated ternary-complex docking, and molecular dynamics simulation. The results identified CLTTMPBA-linker-E7820 as a computationally prioritized PROTAC architecture with favorable predicted binding behavior, residue-level interaction patterns, and simulated ternary-complex stability. Importantly, this study is entirely computational and should be interpreted as an early-stage in silico prioritization framework rather than experimental evidence of BRD4 degradation or anticancer efficacy. The proposed BRD4-DCAF15 PROTAC candidates represent lead hypotheses that require biochemical, cellular, pharmacological, and in vivo validation, including confirmation of target engagement, ternary-complex formation, proteasome-dependent BRD4 degradation, downstream transcriptional modulation, pancreatic cancer cell inhibition, selectivity, pharmacokinetics, toxicity, and antitumor efficacy.

Keywords: Pancreatic cancer, BRD4 oncogenic protein, PROTAC technology, AI-assisted drug design, targeted protein degradation

Introduction

Pancreatic cancer is considered to be one of the most deadly types of cancer in oncology. It is a very aggressive disease with a high risk of early metastasis and with a late diagnosis, which leads to a very poor prognosis [1]. The five year survival rate remains low usually below 12%-raising pancreatic cancer to one of the leading causes of cancer-related mortality in many industrialized countries despite its proportionately low incidence in comparison to other cancers [2, 3]. It is the deadliest with a rate of approx. 94 percent of deaths against incidence in 2023; more than 500,000 people died worldwide. The disease is prevalent among the older adults, with 65-74 years old constituting the most dangerous age group in terms of death [4].

There are minimal therapeutic choices available in the face of pancreatic malignancies and

https://doi.org/10.62347/EKCM7279

majority of patients find themselves at advanced stages at which curative therapy is seldom attainable [5]. The currently available standard-of-care therapies, which include surgical resection, chemotherapy, and radiotherapy, have resulted in only slight improvements in how patients fare, with median survival in patients with metastatic forms of the disease now less than 12 months in most applications [6]. Complex biology, rich stroma, and very immunosuppressive microenvironment in the tumor stall drug delivery and support resistance to treatment. Furthermore, because of non-specific and even lacking early symptoms, late-stage diagnosis is typical which also restricts effective intervention [7, 8].

More recent developments in precision medicine and molecular-targeted drugs have promised results, but the majority of actionable genetic mutations happen in a small subset of patients. The absence of effective methods of early screening and the predictive biomarkers serves as an additional challenge to the timely and effective management of the disease [9, 10].

Set upon this serious burden of the disease, there is a necessity to devise innovative targeted therapies of pancreatic cancer. Novel strategies and innovative treatments, such as proteolysis targeting chimeras (PROTACs), precision oncology, and immuno combinations, are the emerging direction in modern cancer research and give hopes to change survival rates with the help of new therapy [11, 12, 63].

BRD4 (Bromodomain-containing protein 4) is a multi-functional nuclear protein that is known to be an important regulator of gene expression and cell cycle propagation. It is a transcriptional and epigenetic modulator that binds acetylated histones and draws transcription complexes to the chromatin allowing RNA polymerase II to transcribe through the promoter into the body of a gene [13]. Recent evidence has indicated the BRD4 as important contributor to pancreatic cancer progression. In the pancreatic tumor tissues, BRD4 has many times been found to be overexpressed than in normal pancreatic cells. This overexpression is correlated with poor tumor behaviors, increased cell growth, and apoptosis resistance. BRD4 inhibition has been reported to reduce pancreatic cancer cell viability, arrest cell cycle, and sensitize pancreatic cancer cells to chemotherapeutics in vitro [14, 15].

BRD4 is a very attractive drug target in pancreatic cancer because it is a key regulator of the malignant phenotype and many oncogenic pathways. In contrast to other conventional targets, BRD4 is a hotspot where multiple oncogenic pathways intersect and it serves that way as a focal point of epigenetic regulation and transcriptional addiction. BRD4 bromodomains are inhibited by small-molecule drugs, which present beneficial anti-tumor activity by interfering with transcription-related functions of BRD4, but resistance and off-targeting still occur [16]. There are currently no approved BRD4-degrading drugs, and no clearly approved BRD4/BET inhibitor for routine cancer therapy; most BRD4/BET-directed agents remain investigational. However, multiple BET inhibitors have entered clinical trials, including BMS-986158, pelabresib/CPI-0610, ZEN-3694/ZEN-003694, AZD5153, molibresib/GSK525762, OTX015/MK-8628, and others.

TPD has emerged as a fascinating and innovative therapeutic strategy that uses the natural ubiquitin-proteasome pathway (UPS) of the cell to specifically degrade an unwanted disease-associated protein, rather than simply inhibiting its action. PROTACs are bifunctional agents consisting of two different ligands linked together: one ligand to a target protein, and one ligand to an E3 ubiquitin ligase [17]. The PROTACs degrade its target proteins by forming a ternary complex of the target, E3 ligase and PROTAC leading to ubiquitination and degradation of the target protein. Unlike the conventional small-molecule inhibitors, which will probably have an occupancy-based effect and may need continuous interactions with the target, a PROTAC will degrade a target with an event-based catalytic approach, which has the potential to degrade a target at sub-stoichiometric doses and hence reduce off-target consequences [18]. This allows the mechanism as well to target even so called undruggable proteins that lack an enzyme active site binding target such as BRD4 that have major potential in the treatment of cancers and other diseases with otherwise difficult molecular target to attack. Furthermore, via a catalytic process, PROTACs ensure increased potency and specificity and can overcome drug resistance points associat-

ed with conventional inhibitors. Such unique properties have persisted in the therapeutic investigation of PROTACs and further clinical and preclinical success in numerous indications [19, 20].

The problem appears particularly challenging in terms of targeted design of the molecules of PROTAC: several components (the target-binding ligand, the E3 ligase ligand, and the linker) must be tuned to work together in a manner that will be effective (which provides ternary complex formation, cellular permeability, pharmacokinetics, and selectivity) [21]. The traditional trial-and-error drug discovery processes can be quite costly and time-consuming, having problems working within the enormous chemical space and complex structure-activity connections characteristic of PROTACs [22]. The breakthroughs in artificial intelligence (AI) and computational models have presented significant potential in solving such issues by providing more time and more accurate design and been behind the aims at generating optimization cycles [22]. Artificial intelligence (AI) strategies, such as molecular docking, prediction of binding affinity using machine learning, and molecule design with generative models can be used to perform virtual screening and refinement of PROTACs with better efficacy, selectivity and drug-like characteristics [23].

The proposed research would be used to design BRD4-targeting PROTACs as a new form of helping pancreatic cancer with the help of AI-guided design and virtual profiling methodologies. The integrative approach using artificial intelligence and combining computational chemistry and modeling of molecules is aimed at improving the efficacy, selectivity, and drug-like qualities of PROTAC degraders and avoid traditional design limitations in terms of structure-activity relationships and off-target impact. AI application allows predicting molecular interactions quickly and accurately, which helps identify selective and potential degrader architectures that can be adjusted to the specific molecular landscape of pancreatic cancer. This method promises to speed up the discovery process, reduce resource-hungry testing cycles and deliver candidate molecules that have superior therapeutic relevance. The ultimate goal of this study is to make a big step toward the treatment of pancreatic cancer by providing a selective degradation tool that may enhance clinical response, overcome drug resistance, and open the door to individualized, mechanism-specific medicine based on targeting epigenetic regulators such as BRD4.

Accordingly, the present study was designed not to claim clinical efficacy, but to computationally prioritize BRD4-targeting PROTAC candidates within a clinically relevant target class where conventional BET inhibitors have reached clinical testing but BRD4-selective degradation remains an emerging and insufficiently explored therapeutic direction.

Methodology

The overall workflow included protein retrieval and preparation, physicochemical characterization, secondary- and tertiary-structure evaluation, binding-pocket prediction, pharmacophore-based ligand identification, ADMET filtering, protein-ligand docking, interaction analysis, PROTAC assembly, BRD4-DCAF15 protein-protein docking, ternary-complex docking, and molecular dynamics simulation. Candidate prioritization was based on combined pharmacophore fit, ADMET/Lipinski acceptability, docking affinity, molecular interaction quality, linker feasibility, ternary-complex compatibility, and MD-derived structural stability.

Protein structure and sequence retrieval

The three-dimensional structure of BRD4 was retrieved from the Protein Data Bank using PDB ID 3MXF, while the DDB1-DDA1-DCAF15 E3 ligase complex was retrieved using PDB ID 8ROX [24]. The corresponding FASTA sequences were also downloaded from the PDB database for sequence-based analyses [25]. Before downstream modeling, non-essential crystallographic molecules, irrelevant heteroatoms, and water molecules were removed where necessary. Hydrogen atoms were added, missing atoms were checked, and the prepared structures were saved in PDB format for subsequent structural validation, pocket prediction, docking, and ternary-complex modeling [26, 27].

Physicochemical characterization

The FASTA sequences of BRD4 and DCAF15 were submitted to ExPASy ProtParam to calcu-

late protein-level physicochemical descriptors [28, 29]. The recorded parameters included the number of amino acids, molecular weight, theoretical isoelectric point, molecular formula, instability index, aliphatic index, and grand average of hydropathicity. These values were used to compare the size, charge tendency, predicted stability, hydrophobicity, and thermal-stability-related characteristics of BRD4 and DCAF15 before docking and complex modeling.

Secondary-structure prediction

Secondary-structure prediction was performed by submitting the BRD4 and DCAF15 FASTA sequences to PSIPRED [30, 31]. The percentages of α-helices, β-strands, and coil regions were extracted from the output files, together with the corresponding prediction confidence scores [32]. These data were used to evaluate whether the prepared tertiary structures were consistent with sequence-derived secondary-structure tendencies.

Tertiary-structure preparation, validation, and comparison

The tertiary structures of BRD4 and DCAF15 were prepared and evaluated before docking and ternary-complex modeling. AlphaFold-derived confidence indicators, including pLDDT and PAE, were considered to identify structurally reliable and less reliable regions [33, 34]. Backbone stereochemical quality was assessed using Ramachandran plot analysis by recording residues located in favored, allowed, and disallowed regions [35, 36]. In addition, the structures were evaluated using complementary model-quality parameters, including MolProbity-related all-atom geometry, clashscore, poor rotamers, ERRAT non-bonded interaction quality, Verify3D residue-environment compatibility, ProSA/QMEAN global quality estimation, and structural alignment with the corresponding experimental PDB templates. The complete multi-parameter validation results are provided in Supplementary Table 1. Structurally reliable regions were used for interpretation of binding pockets, docking poses, protein-protein interfaces, and ternary-complex stability.

Binding-pocket prediction

The prepared BRD4 and DCAF15 structures were submitted separately to PRANKWEB for ligand-binding-pocket prediction [37]. Predicted pockets were ranked according to pocket score, probability, and number of involved residues [38]. For BRD4, the highest-ranked predicted pocket was used as the primary region for pharmacophore-guided screening and ligand-docking interpretation. For DCAF15, predicted ligandable regions were compared with the reported E7820-binding region to support E3-ligase ligand docking and subsequent interaction analysis.

BRD4 pharmacophore modeling and chemical-library screening

The BRD4-JQ1 complex structure obtained from PDB ID 3MXF was used as the structural template for pharmacophore modeling in Pharmit [39]. The pharmacophore model was generated from the JQ1-binding pocket of BRD4 by selecting the key interaction features required for ligand recognition, including hydrophobic centers, aromatic interaction features, and hydrogen-bond acceptor/donor features. Virtual screening was performed against the PubChem 3D conformer library available through the Pharmit platform. PubChem was selected because it provides a large, structurally diverse, publicly accessible compound collection with compound identifiers that can be directly used for downstream structure retrieval and reproducibility.

During screening, hits were ranked according to pharmacophore-fit quality, shape complementarity, and RMSD relative to the selected pharmacophore features. Only compounds matching the essential BRD4 pharmacophore features and showing low RMSD values were retained for further evaluation. The top-ranked hits were exported with their PubChem compound identifiers and then subjected to 3D-structure retrieval, geometry optimization, ADMET filtering, and molecular docking. The DCAF15-recruiting ligand E7820 was selected from the literature based on its reported ability to engage DCAF15 and was used as the E3-ligase-recruiting moiety for subsequent PROTAC design [40].

Ligand identification and 3D structure preparation from PubChem hits

The chemical source library used for BRD4 ligand screening was the PubChem 3D con-

former library implemented in Pharmit. Therefore, all shortlisted hits were recorded using their PubChem compound identifiers to ensure traceability and reproducibility. The final ten BRD4-binding candidates selected from this library were CTIP, CTTMAA, CLTTMPBA, BCTTOPEP, CTTA2MP, MCTTB, CTPPEE, CTA, CTTAEP, and CTTMPBA. Available 3D conformers were retrieved directly from PubChem, whereas compounds without suitable 3D conformers were generated and energy-minimized in Avogadro before docking [41-45].

ADMET and Lipinski filtering

The shortlisted BRD4 ligand candidates were submitted to ADMETlab 3.0 for prediction of absorption, distribution, metabolism, excretion, toxicity, and drug-likeness-related properties [46, 47]. Lipinski Rule of Five parameters were evaluated together with the broader ADMET profile. Ligands were classified as accepted, partially acceptable, or rejected according to the combined interpretation of ADMET behavior and Lipinski compliance. Because PROTAC precursors and linker-conjugated molecules may deviate from conventional small-molecule drug-likeness space, ADMET/Lipinski results were not used as the only exclusion criterion; instead, they were integrated with docking affinity and molecular interaction quality.

Protein-ligand molecular docking

Prepared BRD4 ligand candidates were docked into BRD4 using CB-Dock2 [48]. The DCAF15 ligand E7820 was docked into the DCAF15 E3 ligase structure using the same docking workflow [49, 50]. For each ligand, the best docking pose was selected according to predicted binding affinity, localization within the predicted binding pocket, absence of severe steric clashes, and preservation of stabilizing interactions. Binding affinities were recorded in kcal/mol. Docking scores were interpreted as computational prioritization indicators rather than direct evidence of biological activity.

Molecular interaction analysis

The best-ranked BRD4-ligand and DCAF15-E7820 docked complexes were analyzed using Discovery Studio Visualizer [51, 52]. The interaction analysis included conventional hydrogen bonds, carbon-hydrogen bonds, π-π stacking, π-alkyl contacts, alkyl interactions, sulfur-mediated contacts, and hydrophobic interactions. Interaction residues, bond types, and interaction distances were recorded. Ligands showing favorable docking affinity, acceptable ADMET/Lipinski behavior, and multiple stabilizing interactions within the BRD4 binding pocket were prioritized for PROTAC assembly.

Scientific rationale for linker design, PROTAC assembly, and 3D modeling

The selected PROTAC was assembled using three components: the BRD4-binding ligand CLTTMPBA, the DCAF15-recruiting ligand E7820, and a linker fragment derived from the reported VH03 linker architecture [21, 53]. The linker was not selected only as a chemical connector, but as a structural element intended to control the spatial orientation, flexibility, solubility, and ternary-complex compatibility of the final PROTAC molecule. In PROTAC design, linker length and composition are critical because they determine whether the target protein and E3 ligase can be brought into a productive proximity suitable for ternary-complex formation and subsequent ubiquitination.

The VH03-derived linker was selected as a rational starting scaffold because it contains flexible ether/PEG-like segments and amide-containing connection points that can provide an appropriate balance between conformational mobility and polar character. The ether-rich segment was used to improve linker flexibility and reduce steric restriction between the BRD4-binding and DCAF15-binding moieties, while the amide connection was retained to provide chemically stable conjugation and maintain a defined ligand-linker geometry. This design was expected to allow the two terminal ligands to orient toward their respective binding regions without forcing a highly strained conformation.

The linker length was chosen to provide sufficient separation between the BRD4 ligand and E7820 while avoiding excessive molecular flexibility that could reduce productive ternary-complex formation. A very short linker may prevent simultaneous engagement of BRD4 and DCAF15 because of steric clashes or incorrect warhead orientation, whereas an excessively long linker may increase entropic penalty, reduce effective local concentration, and weaken

ternary-complex cooperativity. Therefore, the VH03-derived linker was used as a chemically reasonable and literature-supported starting linker for computational PROTAC construction [21, 53].

The BRD4 ligand, E7820, and linker were manually assembled in ChemDraw, and the resulting PROTAC structure was converted into a three-dimensional conformation. The assembled molecule was then energy-minimized in Avogadro to remove unfavorable bond lengths, bond angles, torsional strain, and intramolecular steric clashes before ternary-complex docking [54]. The optimized structure was visually inspected to confirm that the linker maintained reasonable flexibility, that both warheads remained accessible for receptor binding, and that no severe intramolecular collapse occurred. Because this study is computational, the linker should be interpreted as a rationally selected preliminary design rather than an experimentally optimized linker. Further linker-length scanning and experimental structure-activity relationship studies will be required to identify the most effective linker for BRD4 degradation.

BRD4-DCAF15 protein-protein docking

Protein-protein docking between BRD4 and the DDB1-DDA1-DCAF15 E3 ligase complex was performed using HADDOCK. Prepared BRD4 and DCAF15 structures were uploaded as docking components. Docking clusters were evaluated using HADDOCK score, cluster population, fraction of common contacts, interface RMSD, van der Waals contribution, electrostatic contribution, and desolvation energy. The final BRD4-DCAF15 model was selected from the cluster showing favorable score, stable interface convergence, and consistent protein-protein contacts.

PROTAC-mediated ternary-complex docking

The selected BRD4-DCAF15 protein-protein docking model was used as the receptor system for ternary-complex docking. The optimized PROTAC molecule was treated as the ligand and docked into the BRD4-DCAF15 receptor complex using PyRx/AutoDock Vina [55, 56]. Receptor and ligand files were converted into PDBQT format before docking. The final ternary-complex pose was selected according to predicted docking affinity, absence of severe steric clashes, linker orientation, simultaneous engagement of BRD4 and DCAF15 binding regions, and stabilizing interactions at both protein interfaces. The selected ternary complex was further examined in Discovery Studio Visualizer for interaction profiling [57].

Molecular dynamics simulation

The selected BRD4-PROTAC-DCAF15 ternary complex was subjected to molecular dynamics simulation in Schrödinger for 500 ns [58]. The system was prepared using an OPLS-based force field, solvated in an explicit-solvent environment, neutralized with counterions, energy-minimized, equilibrated, and then subjected to production simulation [59, 60]. Stability was evaluated using backbone RMSD, ligand RMSD, residue-wise RMSF, hydrogen-bond persistence, protein-ligand contact occupancy, solvent-accessible surface area, radius of gyration, and interaction-energy components. The MD results were used to assess the dynamic stability of the predicted ternary-complex model and were not interpreted as experimental proof of BRD4 degradation.

Proposed functional verification strategy

Because the present study is based on computational screening and virtual profiling, functional verification is required before the proposed PROTAC candidates can be considered biologically active BRD4 degraders. The computationally prioritized candidate should first be evaluated in pancreatic cancer cell lines, including PANC-1, MIA PaCa-2, AsPC-1, and BxPC-3. Cellular BRD4 degradation should be quantified by Western blotting, capillary immunoassay, HiBiT-BRD4 degradation assay, or targeted quantitative proteomics. Key degradation parameters, including DC50, Dmax, degradation kinetics, and recovery after compound washout, should be determined.

To confirm that BRD4 loss is PROTAC-mechanism dependent, rescue experiments should be performed using proteasome inhibitors such as MG132 or bortezomib, excess BRD4-binding ligand, excess DCAF15-recruiting ligand, and, where feasible, DCAF15 knockdown or knockout. Restoration of BRD4 levels under these conditions would support ubiqui-

tin-proteasome- and DCAF15-dependent degradation. Ternary-complex formation should be validated using NanoBRET, TR-FRET, AlphaScreen, or co-immunoprecipitation assays.

Functional anticancer activity should then be assessed using cell-viability assays, colony-formation assays, apoptosis analysis, cell-cycle analysis, and measurement of BRD4-regulated transcriptional outputs, including MYC-associated signaling. Selectivity should be examined using non-malignant pancreatic ductal epithelial cells and global proteomic profiling to detect off-target degradation. Finally, in vivo validation should be performed in pancreatic cancer xenograft, orthotopic, or patient-derived xenograft models to evaluate pharmacokinetics, biodistribution, tumor BRD4 depletion, downstream pharmacodynamic biomarkers, antitumor efficacy, systemic toxicity, and tolerability.

These experimental steps were not performed in the present study and are therefore proposed as the necessary next stage for biological and translational validation of the computationally prioritized PROTAC candidates.

Results

The results were analyzed using a stepwise prioritization strategy. First, the structural quality of BRD4 and DCAF15 models was evaluated using stereochemical validation and secondary-structure consistency. Second, predicted binding pockets were compared with docking poses to confirm whether ligand binding occurred within plausible ligandable regions. Third, pharmacophore-screened ligands were ranked using RMSD/fitness, ADMET acceptability, Lipinski compliance, and predicted BRD4 binding affinity. Fourth, the best ligand was selected for PROTAC assembly only after considering both docking affinity and interaction quality. Finally, the BRD4-DCAF15 docking model and PROTAC-mediated ternary complex were assessed by HADDOCK cluster behavior and MD-derived stability descriptors.

Targeted protein retrieval

Two protein systems were selected for the computational PROTAC design workflow: BRD4, the target protein associated with pancreatic cancer-related transcriptional regulation, and the DDB1-DDA1-DCAF15 E3 ligase complex, which was used as the E3 ligase recruitment component. The BRD4 structure complexed with JQ1 was retrieved from the Protein Data Bank using PDB ID 3MXF. The DDB1-DDA1-DCAF15 complex was retrieved using PDB ID 8ROX. FASTA sequences corresponding to these structures were downloaded for sequence-based physicochemical and secondary-structure analyses. The prepared structures were then used for validation, binding-pocket prediction, docking, PROTAC assembly, and ternary-complex modeling.

Physicochemical properties of BRD4

To identify the important characteristics of the BRD4 and DCAF15 proteins, the ExPASy ProtParam tool was used to calculate such properties on the basis of primary amino acid sequences. BRD4 is a bromodomain-containing protein involved in pancreatic cancer, and consists of 127 amino acids with an approximate molecular weight of 15.1 kDa and under physiological pH conditions, a theoretical isoelectric point (pI) 7.67, which is close to neutral. It has an instability index (41.59) that signifies borderline-stable and an aliphatic index (76.77) representing a moderate thermostability. The GRAVY score of 0.674, which indicates a rather hydrophobic nature, affects the process of protein folding and the possibility of interaction. On the other hand, DCAF15, an absolutely essential substrate binder in the CUL4-DDB1 E3 ligase complex is many-fold larger (1,541 aa, molecular weight of approximately 171.8 kDa), and has a lower theoretical pI of 5.62. It has an instability index of 43.01 confirming moderate stability and a greater aliphatic index of 84.30 that indicates greater thermal stability as compared to BRD4. The negative GRAVY value (-0.275) indicates a generally hydrophilic character which is quite expected as this protein helps in facilitating protein to protein interactions and also in substrate recognition and recruitment. The presented physicochemical characteristics explain the relevant structural and biochemical attributions that can guide the creation and optimization of PROTAC molecules that target the BRD4-DCAF15 axis (**Table 1**).

Protein secondary structure predictive annotation

PSIPRED secondary structure prediction result is highly informative of the structural composi-

Table 1. Described physicochemical analysis of BRD4 protein and DCAF15 E3 ligase

Protein	No. of AA	Theoretical pI	Molecular weight	Formula	Instability index	Aliphatic index	GRAVY
BRD4	127	7.67	15083.43	$C_{687}H_{1058}N_{174}O_{194}S_7$	41.59	76.77	0.674
DCAF15	1541	5.62	171792	$C_{7624}H_{11947}N_{2071}O_{2312}S_{68}$	43.01	84.30	-0.275

Table 2. Indicated secondary structure characterization of proteins

Protein	Alpha helix	Beta sheets	Coils	Confidence
BRD4	50.63%	49.38%	0%	87.5%
DCAF15				
Chain A	34.3%	28.9%	36.6%	83.3%
Chain B	23.3%	45.4%	31.3%	86.7%
Chain C	45.1%	17.1%	37.8%	90%

tion and confidence level of proteins involved. For BRD4, the protein is predominantly composed of alpha helices and coils that comprise 50.63% and 49.38% of the structure, respectively, and does not contain beta sheets. There is a high confidence level in the prediction overall, which is 87.5%. DCAF15 protein complex has more structural diversity between chains compared to BRD4. Chain A has 34.3% of alpha helices, 28.9% beta sheets, and 36.6% coils with 83.3% confidence. Chain B has lower alpha helix at 23.3%, but higher percentage of beta sheets at 45.4%, and 31.3% coils, with 86.7% confidence. Chain C has 45.1% of alpha helices, 17.1% beta sheets, and 37.8% coils with the highest confidence at 90%. All these indicate the varying secondary structure composition of the DCAF15 complex and form a robust platform for further structural and functional analysis necessary to drug development and protein-targeting actions (**Table 2**).

Validation and elucidation of the tertiary structure

The quality of the BRD4 and DCAF15 structures was assessed using multiple complementary validation methods rather than Ramachandran plot analysis alone. Ramachandran analysis showed that 95.5% of BRD4 residues and 87.5% of DCAF15 residues were located in favored regions, indicating acceptable backbone stereochemistry (**Table 3**). However, because Ramachandran plots evaluate only backbone dihedral-angle geometry, additional validation was performed to assess local confidence, side-chain quality, atomic clashes, residue-environment compatibility, global energetic quality, and similarity to experimentally resolved structures.

AlphaFold confidence analysis was used to examine pLDDT and PAE distributions. High-confidence regions were prioritized for binding-site and docking interpretation, whereas low-confidence flexible loops and terminal regions were interpreted with caution. MolProbity analysis was used to assess steric clashes, rotamer quality, and overall all-atom geometry. ERRAT was used to evaluate the quality of non-bonded atomic interactions, while Verify3D was used to determine whether the three-dimensional environment of each residue was compatible with its amino-acid identity. ProSA-web and/or QMEAN analysis was further used to evaluate the global energetic plausibility of the models. Finally, structural superposition against experimentally available reference structures was performed using PDB IDs 3MXF for BRD4 and 8ROX for the DDB1-DDA1-DCAF15 complex. RMSD and TM-score values were used to confirm whether the prepared models retained the experimentally observed fold.

Ligand binding pocket prediction of BRD4 and DCAF15 ligase

The use of a machine learning method based on PRANKWEB tool for the identification of ligand binding sites in the core of BRD4 and DCAF15 proteins demonstrated that highly reliable results could be obtained to correctly identify these sites. PRANKWEB determines the microchemical characteristics of the surroundings of the protein surface with no usage of templates and attributes to the points of the accessible surface a ligandability score and combines high-scoring points into binding sites that are anticipated. In the case of BRD4, the tool came up with two main active sites, having scores of 12.30 and 1.62, which were corresponding to 13 and 11 residues respectively,

Table 3. Displayed proteins 3D structure and validation

Proteins	PDB ID	3D structure	Validation
BRD4	3MXF	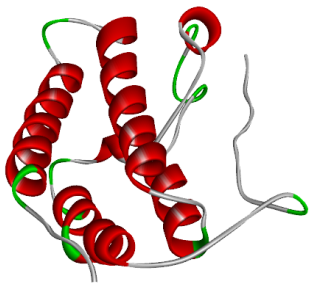	95.5%
DCAF15 Ligase	8ROX	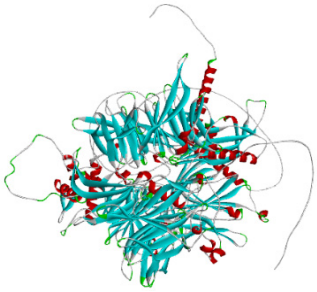	87.5%

Table 4. Demonstrated ligand binding sites values on BRD4 protein

Colors	Rank	Score	Probability	No. of residues
	Site 1	12.30	0.668	13
	Site 2	1.62	0.025	11

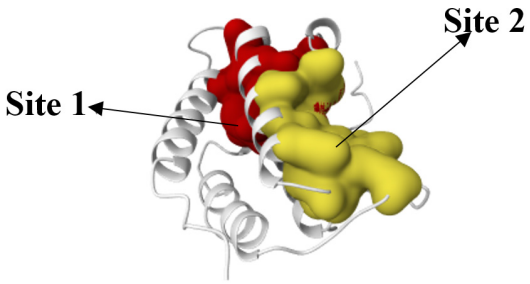

Figure 1. BRD4 protein ligand binding pockets predicted by PRANKWEB online server.

showing high prediction of ligand contact region (**Table 4**; **Figure 1**). DCAF15 has also been predicted to have ten active sites, with the highest scoring site having a score of 27.82 and has 39 interacting residues that show that there are potential multiple sites of ligand binding on DCAF15 protein (**Table 5**; **Figure 2**). PRANKWEB also incorporates sequence conservation analysis along with interaction to determine pockets that are most likely to be correct and to do 3D visualization of result, allowing further verification of predicted pockets.

Pharmacophore profiling of BRD4 protein

A structure-based pharmacophore model was generated using the BRD4-JQ1 complex structure from PDB ID 3MXF. The model retained key BRD4-JQ1 interaction features, including hydrophobic centers, aromatic interaction features, and hydrogen-bond acceptor/donor features (**Figure 3**). Based on these pharmacophore criteria, the PubChem 3D conformer library available through Pharmit was screened to identify BRD4-binding candidates. Compounds matching the essential BRD4 pharmacophore features and showing favorable RMSD/fit values were retained. The top ten hits were exported with their PubChem compound identifiers and used for downstream ADMET profiling, molecular docking, and PROTAC design.

Ligands identification and structure retrieval

Ten BRD4-binding candidates were selected from the PubChem 3D conformer library based on pharmacophore matching, RMSD/fit behavior, and compatibility with the BRD4 binding site. The shortlisted ligands were CTIP, CTTMAA, CLTTMPBA, BCTTOPEP, CTTA2MP, MCTTB, CTPPEE, CTA, CTTAEP, and CTTMPBA (**Table 6**). Available three-dimensional conformers were retrieved directly from PubChem. For compounds without suitable 3D conformers, structures were generated and energy-minimized in Avogadro before docking. This ligand set was then used for ADMET filtering, BRD4 docking, molecular-interaction analysis, and PROTAC construction.

ADMET analysis of ligand candidates

The ADMET results showed that ligand prioritization could not be based only on docking affinity because several ligands showed a mis-

Table 5. Described active sites and residues of DCAF15 E3 ligase

Colors	Rank	Score	Probability	No. of residues
	Site 1	27.82	0.885	39
	Site 2	14.68	0.648	30
	Site 3	12.98	0.588	30
	Site 4	8.35	0.379	15
	Site 5	7.50	0.332	17
	Site 6	6.66	0.285	19
	Site 7	6.66	0.284	18
	Site 8	6.59	0.281	14
	Site 9	4.80	0.175	11
	Site 10	4.75	0.173	14

match between predicted binding strength and drug-likeness behavior. MCTTB, CLTTMPBA, and CTTMPBA satisfied both ADMET and Lipinski criteria and were therefore considered the most balanced candidates from a developability perspective (**Table 7**). CTIP showed strong predicted BRD4 binding but only partial ADMET/Lipinski acceptability, indicating that it may require structural optimization before further development. CTA, BCTTOPEP, and CTTAEP were deprioritized because they failed both ADMET and Lipinski filters, suggesting possible limitations in pharmacokinetic or physicochemical behavior. Therefore, the final candidate selection was based on integrated ADMET-docking performance rather than docking score alone.

Protein-ligand molecular docking analysis

The docking results revealed a clear ranking of BRD4 ligand candidates. CTIP showed the most favorable predicted binding affinity, followed by CLTTMPBA and CTA (**Table 8**). However, CTA was not prioritized because its ADMET and Lipinski behavior were unfavorable. CLTTMPBA was selected as a more balanced BRD4-binding scaffold because it combined strong predicted binding affinity with acceptable ADMET and Lipinski profiles. MCTTB also showed favorable integrated behavior, although its docking score was slightly weaker than CLTTMPBA. Therefore, CLTTMPBA represented the most suitable compromise between binding strength, drug-likeness, and downstream PROTAC design feasibility. This selection strategy reduces the risk of overinterpreting docking energy alone and provides a more rational basis for PROTAC assembly.

Molecular interaction analysis

The best-ranked BRD4-CLTTMPBA and DCAF15-E7820 docked complexes were analyzed using Discovery Studio Visualizer. In the BRD4-CLTTMPBA complex, CLTTMPBA formed conventional and carbon-hydrogen bonds with residues including TYR78, CYS84, ASP87, and PHE42. Additional hydrophobic, π-π, π-alkyl, alkyl, and sulfur-mediated interactions involved residues such as PHE88, MET91, PHE92, LEU30, LEU33, ILE69, and PHE116. These interactions suggest that CLTTMPBA was stabilized within the predicted BRD4 binding pocket through a combination of polar and hydrophobic contacts (**Table 9**). In the DCAF15-E7820 complex, key interactions involving TRP600 and TYR598, including hydrogen bonding and π-π stacking, supported the predicted recognition of E7820 by the DCAF15 binding region. Overall, the interaction profiles supported the selection of CLTTMPBA and E7820 as the BRD4-binding and DCAF15-recruiting moieties, respectively (**Table 10**). These results should be interpreted as predicted molecular-interaction features rather than experimental evidence of target engagement or degradation activity.

PROTAC assembly and 3D modeling

The final PROTAC architecture was assembled using CLTTMPBA as the BRD4-binding moiety, E7820 as the DCAF15-recruiting moiety, and a VH03-derived linker as the connecting scaffold. The linker was selected to provide sufficient spatial separation between the two terminal ligands while maintaining conformational flexibility through its ether-rich segment and chemical stability through amide-containing connection points. The ligand-linker-ligand structure was constructed in ChemDraw and converted into a three-dimensional conformation. The assembled PROTAC was energy-minimized in Avogadro to reduce unfavorable bond lengths, torsional strain, and intramolecular steric clashes before ternary-complex docking. The optimized structure showed a ligand-linker-ligand architecture compatible with the intended BRD4-DCAF15 recruitment strategy. However, the linker should be considered a rational preliminary design and requires future

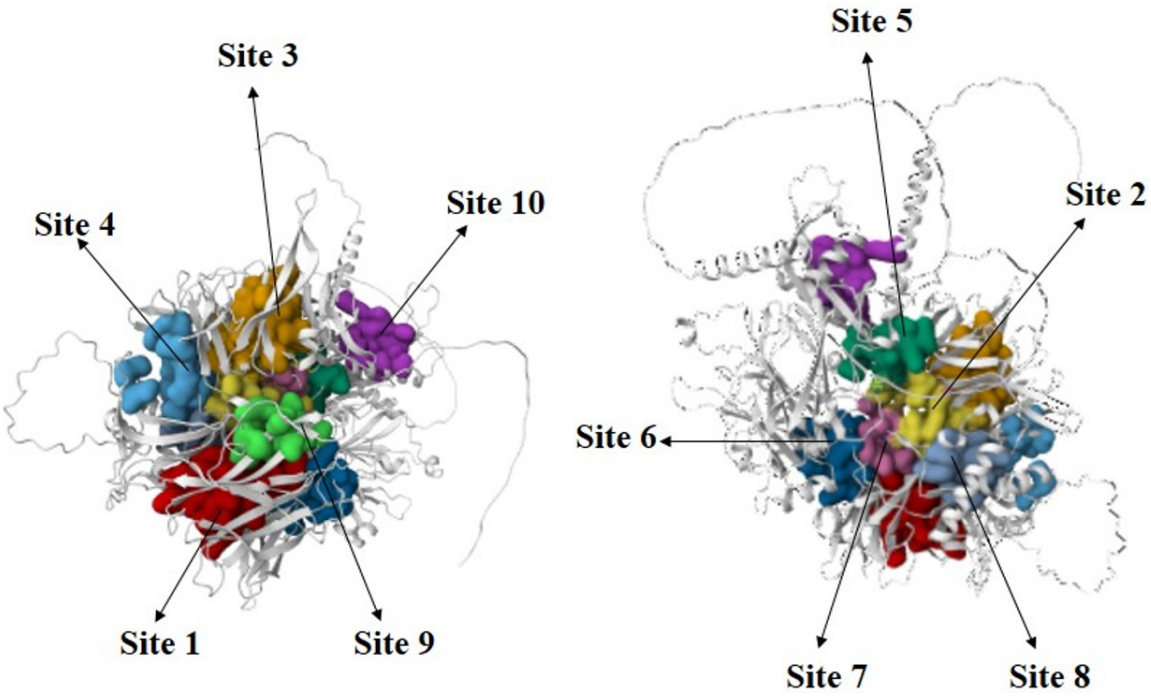

Figure 2. DCAF15 E3 ligase ligand binding pockets predicted by PRANKWEB online server.

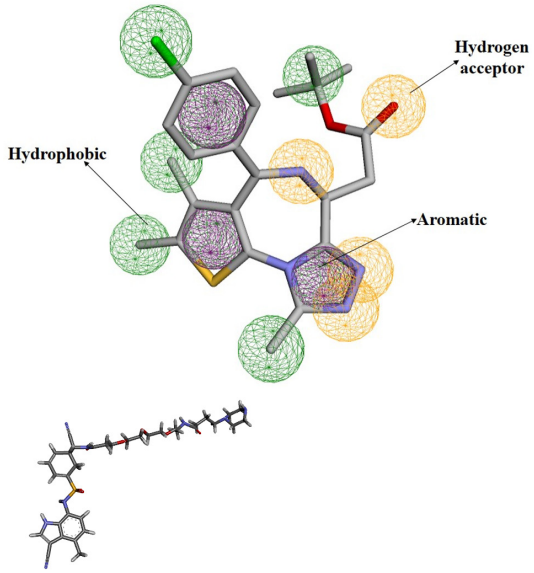

Figure 3. BRD4 JQ1 pharmacophore structure predicted by pharmit online tool.

linker-length and attachment-vector optimization.

Molecular docking and cluster analysis of BRD4-DCAF15 complex

Protein-protein docking was performed to generate a plausible BRD4-DCAF15 spatial arrangement for subsequent PROTAC-mediated ternary-complex modeling. HADDOCK produced multiple docking clusters, which were evaluated using HADDOCK score, fraction of common contacts, interface RMSD, van der Waals contribution, electrostatic contribution, and restraint-energy behavior. Cluster 2 showed the most favorable overall profile, including a low HADDOCK score, high fraction of common contacts, compact interface-RMSD distribution, and favorable interaction-energy components. The high fraction of common contacts indicated that the docked poses within this cluster shared a consistent interaction interface, while the low interface-RMSD values suggested structural convergence. Therefore, Cluster 2 was selected as the BRD4-DCAF15 receptor model for PROTAC-mediated ternary-complex docking (**Figure 4**). This result represents a predicted structural arrangement for computational modeling and does not confirm spontaneous BRD4-DCAF15 association experimentally.

Haddock predicted results plot explanation

The first graph shows the correlation between the defined HADDOCK scores and the fraction of common contacts (FCC) of protein-protein

Table 6. Showed BRD4 protein ligands and their 3D structures with PubChem ID

Sr. No.	Ligands	PubChem	RMSD	3D structures
1	CTIP	160563288	0.543	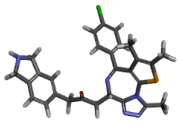
2	CTTMAA	68199839	0.412	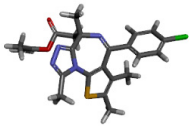
3	CLTTMPBA	118178847	0.412	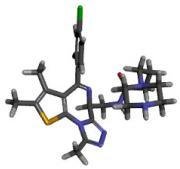
4	BCTTOPEP	158014728	0.387	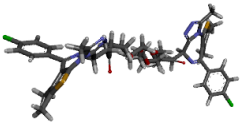
5	CTTA2MP	118595663	0.384	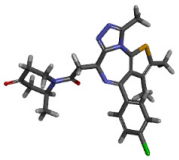
6	MCTTB	146037626	0.378	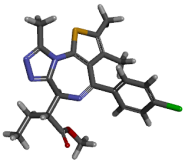
7	CTPPEE	163671012	0.086	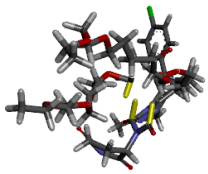
8	CTA	158901943	0.64	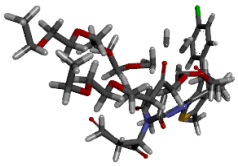
9	CTTAEP	157290077	0.368	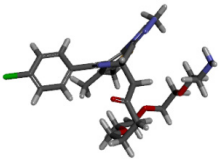
10	CTTMPBA	118178847	o.357	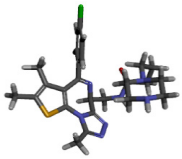

docking clusters. The most promising cluster of HADDOCK is cluster 2, with the lowest average score of HADDOCK -85 (greater binding affinity) accompanied by a favorable and large FCC closest to 0.8 signifying uniform and dependable docking modes in this cluster. The fact that this has been found denotes that Cluster 2 is the most stable and biologically significant interaction model. The HADDOCK docking results and cluster-analysis plots are shown in **Figure 5**.

The second graph shows the values of HADDOCK scores against interface-RMSD with respect to various docking clusters of the protein-protein complex. Cluster 2 presents the most favorable cluster with the lowest HADDOCK score with an average of -85 which points to the best binding energy. It also has a great consistency in terms of docking poses, and the interface-RMSD values are relatively low, which indicates the reliability of structures. The good score and the high concentration of points around low values of RMSD makes Cluster 2 the most stable and biologically relevant of the found clusters of the docking conformation.

The third graph is the plot of HADDOCK scores, against the interface RMSD of several docking clusters in the protein complex. However, one can see that cluster 2 is obviously the best cluster, with the lowest mean HADDOCK score of approximately -85, which signifies the highest binding affinity. It also indicates that the interface-RMSD values are narrow with most of the values below

Table 7. Represented ADMET profiling of all BRD4 ligand candidates

Ligands	ADMET profile	Lipinski Rule	Ligands	ADMET profile	Lipinski Rule
CTIP	Partial acceptable	Partial acceptable	MCTTB	Accepted	Accepted
CTTMAA	Rejected	Accepted	CMTT-PE	Rejected	Accepted
CLTTMPBA	Accepted	Accepted	CTA	Rejected	Rejected
BCTTOPEP	Rejected	Rejected	CTTAEP	Rejected	Rejected
CTTA2MP	Rejected	Accepted	CTTMPBA	Accepted	Accepted

Table 8. Indicated binding affinities of BRD4-ligands docked complexes

Ligands	Binding affinity	Ligands	Binding affinity
CTIP	-10.4	MCTTB	-9.1
CTTMAA	-8.1	CMTT-PE	-7.4
CLTTMPBA	-9.7	CTA	-9.7
BCTTOPEP	-7.3	CTTAEP	-6.5
CTTA2MP	-8.9	CTTMPBA	-8.3

2 which indicates structural consistency and reproducibility of docking poses. Cluster 2 is the most relevant and steady docking model to be utilized in docked form since it has a low score and clustered close together.

The fourth graph indicates the dependence between the van der Waals energy (Evdw) and interface-RMSD measured on various clusters. Cluster 2 is the most favorable cluster with the majority of the points being the most favorable (having the lowest values of interface-RMSD (minimum close to 0-2) and the lowest van der Waals energies (as low as -80), showing that the connection of mutated amino acids is the best. The difference in I-RMSD between Cluster 1 and 3 is also relatively low but in comparison, there is relatively higher (less negative) Evdw value in Clusters 1 and 3. The interface-RMSD between cluster 4, 5 and 6 is larger with a worse energy range indicating weaker or inaccurate interaction possibly due to the larger interface.

The interface-RMSD versus the electrostatics energy relationship is illustrated on this graph fifth over distinct clusters. The cluster 2 has the best performance, with most of its points depicting good interface-RMSD (approximating to 0-2) and extremely appealing electrostatics energies (going down to about 350). Other clusters in 1 and 3 contain a slight increase in I-RMSD and less negative values in electrostatics energies whereas the worst is in cluster 4, 5, and 6 with higher i-RMSD scores (closer to 8-12) and lesser-favored energies. The particular cluster 2 therefore presents the most structural accuracy and the strongest interaction in this comparison.

The sixth graph indicates the correlation between restraint ranks energy and interface-RMSD of various clusters. Cluster 2 emerges as the superior one with the points that are closely clustered together with low interface-RMSD values (0-2) as well as low restraint energies which have a range of 200-300. The rest of the clusters like 4 and 5 show the higher degree of I-RMSD (approximately 12) and restraint energies which is worse. Closure Cluster 2 has both the best structural fit and energy values in this analysis therefore denoting it as accurate and recommendable of the structural model of the other clusters.

The seventh boxplot describes the spread of van der Waals energy among various clusters on the basis of which the different clusters are marked along the x-axis. Cluster 2, (which has the most favorable values of van der Waals energy in this case having the least negative values meaning most favorable) has the median energies of -35, which is very larger than in the other clusters. This finding indicates that the Cluster 2 structures are potentially favorable energetically due to van der Waals interactions.

The eighth boxplot illustrates the value of distribution of electrostatics energy with its different clusters, which is plotted on the x-axis. Cluster 2 will have the highest values of electrostatics energy (not most negative), which makes it the most favourable group of molecules in terms of the electrostatic interactions with energy values centred at around -170. This can mean that the structures in Cluster 2 can be more electrostatically stable than the rest.

Table 9. Molecular interaction profile of the selected BRD4-CLTTMPBA complex

BRD4 protein with CLTTMPBA						
Sr. No	Residues	Bond type	Distance	Residues	Bond type	Distance
1	:UNK0:H50 - B:TYR78:OH	Conventional Hydrogen Bond	2.42699	B:PHE92 - :UNK0	Pi-Pi Stacked	3.39627
2	:UNK0:H50 - B:CYS84:O	Conventional Hydrogen Bond	2.90139	:UNK0:CL1 - B:MET91	Alkyl	5.28091
3	:UNK0:H55 - :UNK0:N9	Conventional Hydrogen Bond	2.55409	:UNK0:C29 - B:MET91	Alkyl	4.43959
4	:UNK0:H41 - B:ASP87:O	Carbon Hydrogen Bond	2.34844	:UNK0:C30 - B:LEU30	Alkyl	3.86344
5	:UNK0:H43 - B:CYS84:O	Carbon Hydrogen Bond	2.74385	:UNK0:C30 - B:ILE69	Alkyl	4.1676
6	:UNK0:H45 - B:TYR78:OH	Carbon Hydrogen Bond	2.9531	:UNK0:C31 - B:LEU33	Alkyl	3.57199
7	:UNK0:H46 - B:TYR78:OH	Carbon Hydrogen Bond	3.06231	B:PHE88 - :UNK0:C29	Pi-Alkyl	5.42815
8	:UNK0:H53 - B:PHE42:O	Carbon Hydrogen Bond	2.21099	B:PHE88 - :UNK0:C31	Pi-Alkyl	4.64934
9	:UNK0:H54 - B:PHE42:O	Carbon Hydrogen Bond	2.26778	B:PHE92 - :UNK0:CL1	Pi-Alkyl	4.86248
10	B:MET66:SD - :UNK0:N6	Sulfur-X	3.05465	B:PHE92 - :UNK0:C31	Pi-Alkyl	4.13869
11	B:ILE69:CD1 - :UNK0	Pi-Sigma	3.12911	B:PHE116 - :UNK0:C31	Pi-Alkyl	3.41266
12	B:MET91:SD - :UNK0	Pi-Sulfur	4.71293	:UNK0 - B:MET66	Pi-Alkyl	4.71297
13	B:MET91:SD - :UNK0	Pi-Sulfur	4.60723	:UNK0 - B:LEU30	Pi-Alkyl	4.76132

Table 10. Displayed molecular interactions between DCAF15 E3 ligase and E7820 ligand

DCAF15 with E7820 ligand			
Sr. No	Residues	Bond type	Distance
1	A:TRP600:NE1 - A:UNL1:O	Conventional Hydrogen Bond	3.09746
2	A:UNL1:H - A:UNL1:O	Conventional Hydrogen Bond	2.65128
3	A:TYR598 - A:UNL1	Pi-Pi Stacked	4.03523
4	A:TRP600 - A:UNL1	Pi-Pi Stacked	4.8904
5	A:TRP600 - A:UNL1	Pi-Pi Stacked	3.84229
6	A:TRP600 - A:UNL1	Pi-Pi Stacked	3.91724
7	A:UNL1 - A:TRP600	Pi-Pi Stacked	3.90876

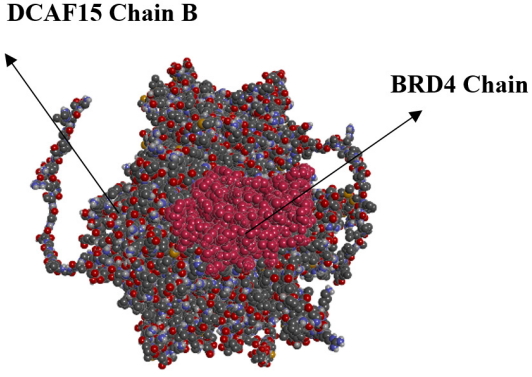

Figure 4. Displayed haddock best complex of BRD4-DCAF15 E3 ligase.

The ninth graph illustrates the correlation between one (HADDOCK score) and the other (Fraction of Common Contacts (FCC)) amongst different clusters. Cluster 2 shows the best FCC near 1.0 and thus worst HADDOCK scores near -100, this is the richest in the best (lowest-scoring, most consistent) models. This finding indicates that Cluster 2 is the highest scoring and contact similar as well.

The HADDOCK cluster analysis indicated that Cluster 2 provided the most suitable BRD4-DCAF15 docking model for subsequent ternary-complex docking. This cluster showed a favorable HADDOCK score, high fraction of common contacts, compact interface-RMSD distribution, and favorable interaction-energy components. The high fraction of common contacts suggested that poses within this cluster shared a consistent interaction interface rather than representing random docking orientations. The low interface-RMSD range further indicated structural convergence among the docked poses. Therefore, Cluster 2 was selected as the receptor model for PROTAC-mediated ternary-complex construction. Importantly, this result should be interpreted as a predicted structural arrangement suitable for computational modeling, not as experimental confirmation of spontaneous BRD4-DCAF15 association.

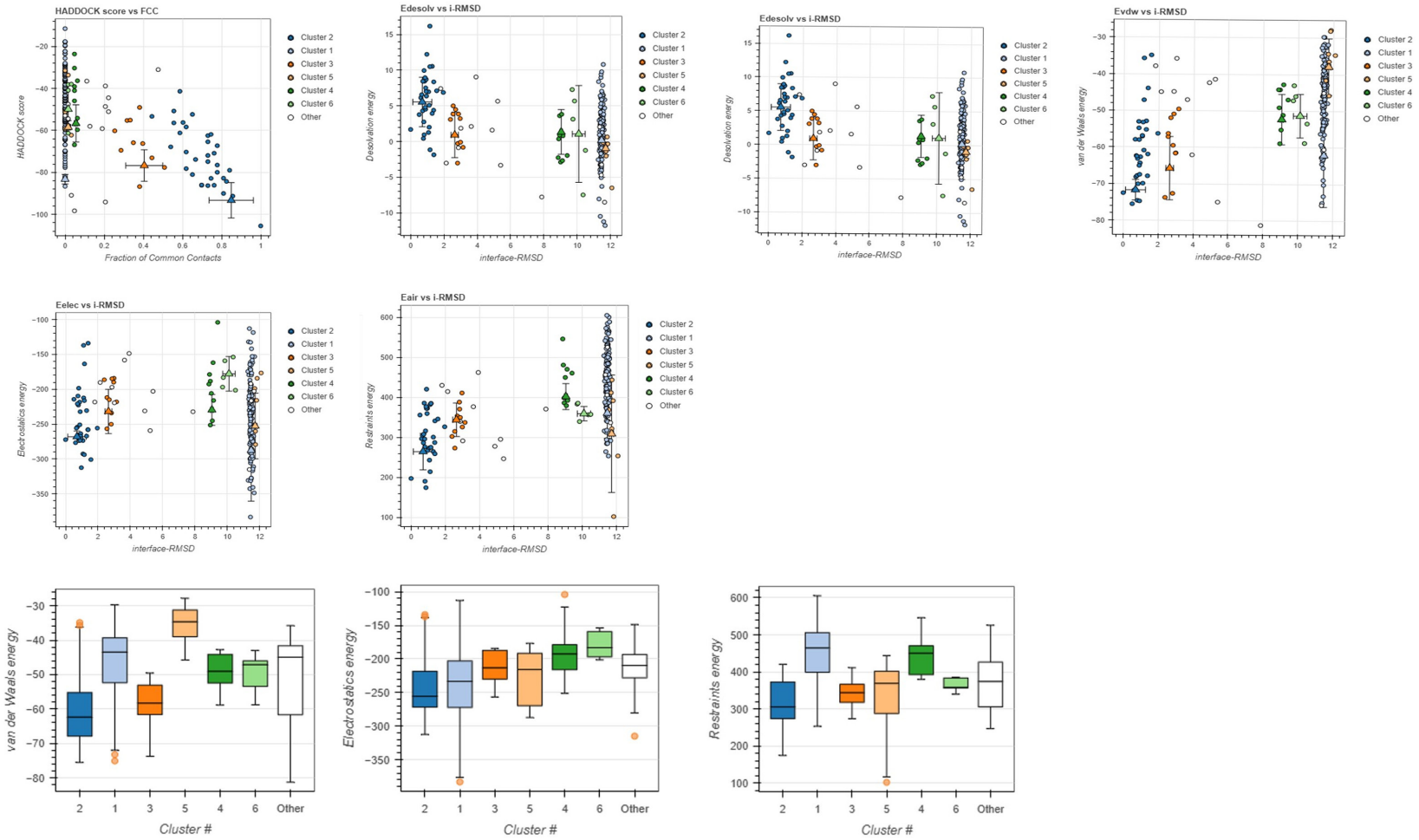

Figure 5. BRD4-DCAF15 docking results graph predicted by HADDOCK server.

Table 11. Describing ternary complex molecular interaction analysis

	Residues	Bond Category	Bond type	Distance
1	Chain A:SER570:HG - Chain L:UNL1:N	Hydrogen Bond	Conventional Hydrogen Bond	2.68509
2	Chain A:ASN1269:HD21 - Chain L:UNL1:O	Hydrogen Bond	Conventional Hydrogen Bond	2.43474
3	Chain A:ARG1379:HH11 - Chain L:UNL1:N	Hydrogen Bond	Conventional Hydrogen Bond	2.93904
4	Chain L:UNL1:C - Chain A:ARG714:O	Hydrogen Bond	Carbon Hydrogen Bond	2.51737
5	Chain A:GLU1378:OE1 - Chain L:UNL1	Hydrogen Bond	Pi-Anion	3.5836
6	Chain A:ASN1269:HD22 - Chain L:UNL1	Electrostatic	Pi-Donor Hydrogen Bond	3.71306
7	Chain A:GLU1378:HN - Chain L:UNL1	Hydrogen Bond	Pi-Donor Hydrogen Bond	3.20205
8	Chain A:UNL1 - Chain P:PRO54	Hydrogen Bond	Pi-Alkyl	3.26195
9	Chain A:UNL1 - Chain P:ALA1270	Hydrophobic	Pi-Alkyl	4.99526
10	Chain A:SER570:HG - Chain L:UNL1:N	Hydrophobic	Conventional Hydrogen Bond	4.8334
11	Chain A:ASN1269:HD21 - Chain L:UNL1:O	Hydrogen Bond	Conventional Hydrogen Bond	2.68509

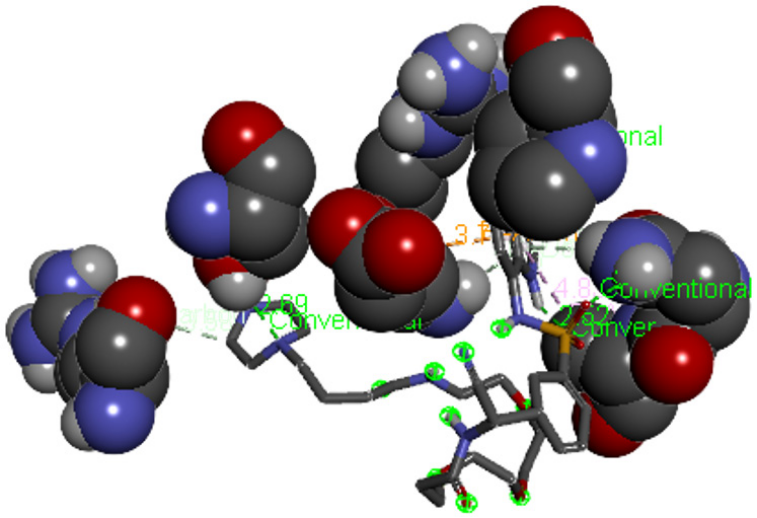

Figure 6. BRD4-DCAF15-PROTAC 3D structure complex interaction analysis.

Ternary complex docking

The BRD4-DCAF15 docking model selected from HADDOCK analysis was used as the receptor system for PROTAC-mediated ternary-complex docking in PyRx/AutoDock Vina. The optimized CLTTMPBA-linker-E7820 PROTAC was treated as the ligand. The docking grid was centered at X = 25, Y = 45, and Z = 32, with a grid size of 25 Å along each axis. The best docking pose showed a predicted Vina score of -9.4 kcal/mol. The selected ternary pose was further analyzed in Discovery Studio Visualizer. The interaction profile showed hydrogen-bond interactions involving residues such as SER570, ASN1269, and ARG1379, as well as π-anion, π-donor hydrogen-bond, π-alkyl, hydrophobic, and electrostatic contacts involving residues such as GLU1378, ASN1269, PRO54, and ALA1270 (**Table 11**). These interactions suggest that the PROTAC can computationally bridge the BRD4-DCAF15 interface in a geometrically feasible orientation (**Figure 6**). However, the docking result should be interpreted as structural support for ternary-complex feasibility, not as confirmation of ubiquitination or proteasomal degradation.

Molecular dynamic simulation

The selected BRD4-PROTAC-DCAF15 ternary complex was subjected to 500 ns molecular dynamics simulation under an NPT ensemble at 310 K (**Figure 7**). The simulated system contained 182,220 atoms, including 51,897 water molecules, 1668 protein residues, and a 99-atom ligand. The total system charge was -33. The protein backbone RMSD reached a stable range of approximately 1-3 Å, indicating that the overall complex remained structurally equilibrated during the simulation. Ligand RMSD relative to the protein backbone remained comparatively low, suggesting that the PROTAC did not undergo major displacement from the modeled binding region.

RMSF analysis indicated that the highest local flexibility occurred mainly in loop and terminal regions, whereas secondary-structure elements and ligand-interface residues remained

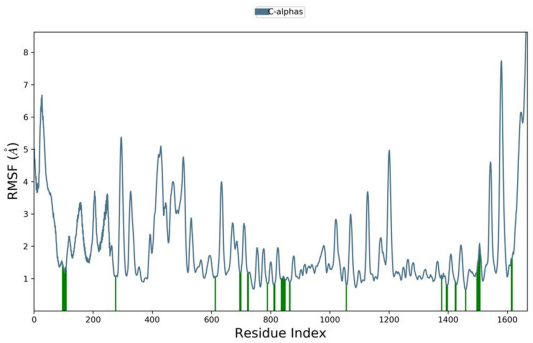

Protein RMSF plot

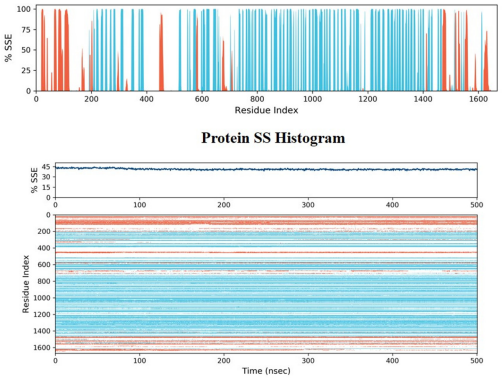

Protein SS Histogram

Protein Timeline

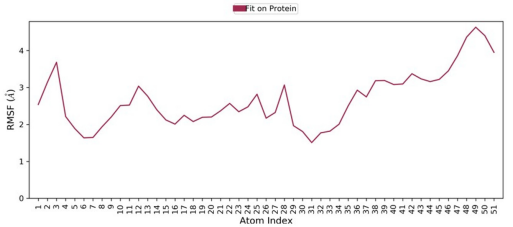

PROTAC (Ligand) RMSF plot

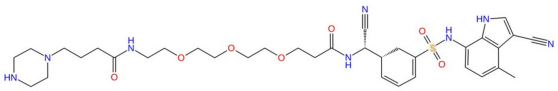

PROTAC (Ligand) Torsion 2D structure

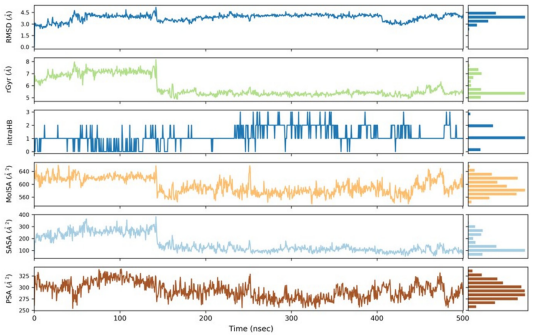

PROTAC (Ligand) properties

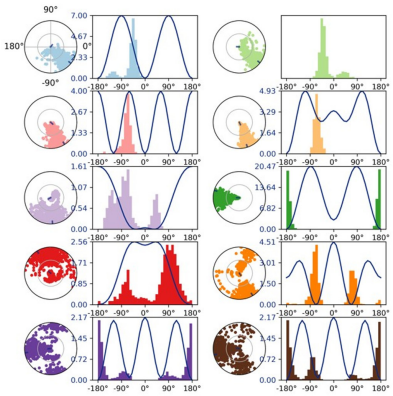

PROTAC (Ligand) Torsion profile

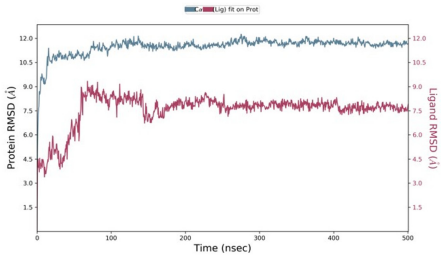

PROTAC-PROTEIN RMSD plot

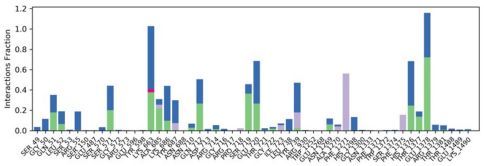

PROTEIN-PROTAC contact

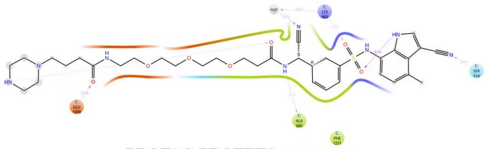

PROTAC-PROTEIN contact

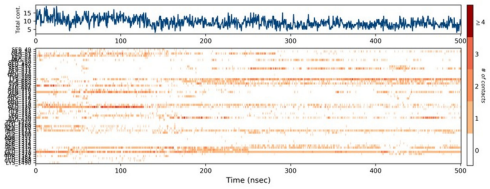

PROTAC-PROTEIN contact Timeline

Figure 7. Displayed MD simulation results graph, histogram, timelines and torsion profiles.

comparatively stable. Secondary-structure analysis showed a stable overall composition, with approximately 41.2% total secondary-structure content, including 8.5% α-helices and 32.7% β-strands. Ligand RMSF and torsional analysis further suggested that the PROTAC maintained a stable conformation without excessive torsional strain. Persistent protein-ligand contacts, including hydrogen bonds, hydrophobic interactions, ionic interactions, and water bridges, were observed during the trajectory. Residues such as GLU487, LYS663, and ARG714 showed long-duration contacts with the ligand, supporting the predicted stability of the complex.

Comparative summary of docking results obtained using different computational tools

To improve clarity, the docking results obtained from different computational tools were compared and summarized according to their specific purpose in the PROTAC design workflow. Because CB-Dock2, HADDOCK, PyRx/AutoDock Vina, and Discovery Studio use different scoring schemes and evaluate different molecular systems, their numerical scores should not be directly compared as equivalent binding-energy values. Instead, the results were interpreted comparatively based on whether each tool supported the same prioritization trend: stable BRD4 ligand binding, DCAF15 recruitment, feasible BRD4-DCAF15 spatial organization, and compatible PROTAC-mediated ternary-complex formation (Supplementary Table 2).

Discussion

Pancreatic cancer remains a highly challenging malignancy because of late diagnosis, aggressive progression, dense stromal architecture, therapy resistance, and limited durable responses to currently available therapeutic strategies [6-12]. These clinical limitations justify continued investigation of molecularly targeted and mechanism-driven approaches. BRD4 is a transcriptional and epigenetic regulator involved in chromatin-dependent gene expression, DNA damage response, transcriptional elongation, and oncogenic signaling [13-16]. In pancreatic cancer, BRD4 has been associated with malignant transcriptional programs that support proliferation, survival, and resistance-related phenotypes [14-16]. Therefore, BRD4 represents a rational target for therapeutic intervention. However, conventional BET/BRD4 inhibition is occupancy-driven and reversible, meaning that inhibition depends on sustained target engagement and may not fully eliminate BRD4-mediated scaffolding or transcriptional functions [16, 18, 22]. This provides the scientific basis for exploring BRD4 degradation as an alternative strategy.

Targeted protein degradation using PROTACs offers a mechanistically distinct approach by recruiting an E3 ubiquitin ligase to a protein of interest and promoting ubiquitin-proteasome-mediated degradation [17-19]. Unlike classical inhibitors, PROTACs depend not only on binary target binding but also on productive ternary-complex formation among the target protein, PROTAC molecule, and E3 ligase [18, 21, 22]. This makes PROTAC design more complex than conventional inhibitor design. The target-binding ligand, E3-ligase-recruiting ligand, linker length, linker chemistry, attachment vector, ternary-complex geometry, cellular permeability, pharmacokinetic behavior, and degradation selectivity must all be considered simultaneously [21-23, 59, 60, 67]. Recent reviews and computational studies have emphasized that PROTAC activity is strongly influenced by ternary-complex stability, cooperativity, linker flexibility, and induced protein-protein interface formation rather than binding affinity alone [59-61, 66, 69].

Previous BRD4-related studies have mainly focused on BRD4 biology, BET bromodomain inhibition, or established PROTAC strategies using commonly exploited E3 ligases such as CRBN or VHL [14-16, 61, 68, 70]. These studies have established the feasibility of targeting BRD4-dependent oncogenic transcription, but they also highlight important limitations, including reversible inhibition, toxicity, resistance, and the need for more rational degrader optimization [18, 22, 61, 68]. In comparison, the present study investigated a DCAF15-recruiting BRD4 PROTAC design strategy. This is relevant because expanding E3-ligase recruitment beyond frequently used CRBN/VHL systems may broaden the degrader-design space and provide alternative opportunities for tissue-, context-, or target-dependent optimization [40, 61, 62, 69]. Thus, the present study contributes not by experimentally proving BRD4 degradation, but by providing a computationally

structured workflow for prioritizing a DCAF15-oriented BRD4 PROTAC architecture.

Compared with previous empirical PROTAC optimization approaches, the main strength of the present study is the integration of multiple computational levels into a single prioritization pipeline. The workflow combined structural retrieval and validation, physicochemical characterization, secondary-structure prediction, binding-pocket mapping, pharmacophore-based screening, PubChem-based ligand traceability, ADMET/Lipinski filtering, binary protein-ligand docking, molecular-interaction profiling, rational linker selection, BRD4-DCAF15 protein-protein docking, PROTAC-mediated ternary-complex docking, and 500 ns molecular dynamics simulation. This multistage design is consistent with recent recommendations that PROTAC optimization should move beyond single docking scores and incorporate structural modelling, pharmacophore analysis, ADMET prediction, linker evaluation, ternary-complex modelling, and dynamic stability assessment [23, 59, 60, 64, 65, 73].

The structural analyses supported the suitability of BRD4 and DCAF15 as receptor systems for downstream virtual screening and docking. BRD4 showed 127 amino acids, a molecular weight of approximately 15.08 kDa, theoretical pI of 7.67, and a GRAVY value of 0.674, whereas DCAF15 showed 1541 amino acids, a molecular weight of approximately 171.79 kDa, theoretical pI of 5.62, and a GRAVY value of -0.275. These physicochemical differences are consistent with the compact bromodomain nature of BRD4 and the larger multidomain architecture of the DCAF15 E3 ligase complex. Ramachandran plot validation showed 95.5% favored residues for BRD4 and 87.5% favored residues for DCAF15, supporting acceptable backbone stereochemistry. In addition, the expanded multi-parameter validation summarized in Supplementary Table 1 further supports the structural reliability of both models before docking. Such multi-level structural assessment is important because unreliable receptor geometry can propagate errors into pocket prediction, docking, ternary-complex modeling, and MD interpretation [33-38].

The pharmacophore-screening and docking analyses showed that ligand prioritization should not be based only on the most negative docking score. CTIP showed the strongest predicted BRD4 binding affinity of -10.4 kcal/mol, whereas CLTTMPBA and CTA showed predicted binding affinities of -9.7 kcal/mol. However, CTA was not favored because of poor ADMET/Lipinski behavior, and CTIP showed only partial acceptability. CLTTMPBA was therefore selected as a more balanced BRD4-binding scaffold because it combined strong predicted binding affinity with acceptable ADMET and Lipinski profiles. This integrated selection strategy is more technically justified than selecting the top docking-score ligand alone, because PROTAC candidates must retain both binding potential and developability-related properties [22, 23, 46, 47, 59]. MCTTB and CTTMPBA also showed acceptable profiles, but CLTTMPBA provided the most suitable compromise for downstream PROTAC construction.

Residue-level interaction analysis further supported the selection of CLTTMPBA as the BRD4-binding moiety. The BRD4-CLTTMPBA complex showed stabilizing hydrogen-bond, hydrophobic, π-π, π-alkyl, alkyl, and sulfur-mediated interactions involving residues such as TYR78, CYS84, ASP87, PHE42, PHE88, MET91, PHE92, LEU30, LEU33, ILE69, and PHE116. These contacts suggest that CLTTMPBA was retained within the BRD4 binding environment through a combination of polar and non-polar interactions. Similarly, the DCAF15-E7820 complex showed key interactions involving TRP600 and TYR598, including hydrogen-bonding and aromatic stacking interactions. These interactions support the use of E7820 as the DCAF15-recruiting moiety. However, these results should be interpreted as predicted molecular-recognition features rather than experimental proof of target engagement or intracellular degradation.

The linker design is another critical component of the proposed PROTAC architecture. Previous studies have shown that linker length, flexibility, polarity, and attachment vectors strongly affect ternary-complex geometry, ubiquitination efficiency, and degradation selectivity [21, 59, 60, 66, 69, 71]. In the present study, a VH03-derived linker was used as a rational starting scaffold because ether/PEG-like segments can provide conformational flexibility and polar character, while amide-containing connection

points can support chemical stability and defined ligand-linker orientation. This design was intended to provide sufficient separation between the BRD4-binding ligand and the DCAF15-recruiting E7820 moiety while avoiding excessive flexibility that could increase entropic penalty and reduce productive ternary-complex formation. This approach is consistent with recent PROTAC design strategies emphasizing linker-guided spatial orientation and dynamic ternary-complex compatibility [59, 60, 66, 69]. Nevertheless, the linker remains preliminary and requires future linker-length scanning, attachment-vector optimization, synthesis, and functional degradation testing.

The docking workflow also differs from studies relying only on binary docking. Binary docking with CB-Dock2 was first used to prioritize BRD4-binding ligands and DCAF15-E7820 recognition. HADDOCK was then used to evaluate possible BRD4-DCAF15 protein-protein arrangements. Cluster 2 showed the most favorable overall protein-protein docking behavior, with a low HADDOCK score, favorable fraction of common contacts, and low interface-RMSD distribution, suggesting a convergent and structurally plausible BRD4-DCAF15 arrangement. PyRx/AutoDock Vina was then used to assess whether the assembled CLTT-MPBA-linker-E7820 PROTAC could bridge the BRD4-DCAF15 model without severe steric conflict. Discovery Studio interaction analysis provided residue-level interpretation of the selected ternary pose. This multi-tool strategy is technically useful because different docking tools provide complementary outputs and should not be interpreted as directly interchangeable binding-energy measurements [23, 49, 55-57, 59, 65].

The 500 ns MD simulation provided a post-docking dynamic assessment of the selected BRD4-PROTAC-DCAF15 ternary complex. The reported backbone RMSD range of approximately 1-3 Å, persistent ligand contacts, limited interface fluctuations, stable secondary-structure behavior, and favorable estimated binding free energy suggest that the selected ternary pose remained structurally stable during the simulation period. These findings are consistent with recent studies emphasizing the need to evaluate PROTAC-induced structural dynamics and ternary-complex persistence rather than relying only on static docking poses [59, 60, 66, 73]. Nevertheless, MD stability does not confirm biological activity. It only indicates that the predicted complex did not undergo major destabilization under the simulated conditions.

The present study demonstrates the utility of an integrated computational workflow for prioritizing BRD4-DCAF15 PROTAC candidates before synthesis and biological testing. The workflow combines target-structure evaluation, pharmacophore screening, ADMET filtering, binary docking, residue-level interaction profiling, linker rationale, protein-protein docking, ternary-complex docking, and MD-based stability assessment. However, these analyses provide structural and computational evidence only. They do not establish cellular uptake, target engagement, ubiquitination, proteasome-dependent BRD4 degradation, anticancer efficacy, pharmacokinetic suitability, or in vivo safety. Therefore, the principal contribution of this work is the generation of experimentally testable BRD4-targeting PROTAC hypotheses, not confirmation of therapeutic activity. Controlled delivery approaches, including nanoparticle-based PROTAC formulations, may further improve intracellular delivery, pharmacokinetic behavior, and therapeutic applicability [72].

Limitations and future experimental validation

The present study provides an AI-assisted computational prioritization workflow for BRD4-targeting PROTAC design; however, the proposed candidates have not yet been experimentally validated in biochemical assays, pancreatic cancer cell lines, or animal models. Therefore, docking scores, ADMET predictions, protein-protein docking results, ternary-complex modeling, MM-GBSA estimation, and MD-derived stability parameters should be interpreted as predictive indicators of structural feasibility rather than direct evidence of biological activity.

In particular, the present results do not confirm cellular permeability, intracellular target engagement, productive BRD4-PROTAC-DCAF-15 ternary-complex formation, BRD4 ubiquiti-

nation, proteasome-dependent BRD4 degradation, downstream transcriptional suppression, cancer-cell growth inhibition, pharmacokinetic suitability, toxicity profile, or in vivo antitumor efficacy. These biological functions require direct experimental validation.

Future work should therefore include a staged functional verification strategy. First, biochemical and biophysical assays should confirm BRD4 binding, DCAF15 recruitment, and ternary-complex formation. Second, cellular assays should determine whether the candidate induces BRD4 degradation in pancreatic cancer cells and whether degradation is rescued by proteasome inhibition, competitive ligand treatment, or DCAF15 suppression. Third, functional assays should assess cell viability, apoptosis, cell-cycle arrest, clonogenic survival, and BRD4-regulated transcriptional changes. Finally, in vivo studies using pancreatic cancer xenograft, orthotopic, or patient-derived xenograft models should evaluate pharmacokinetics, pharmacodynamics, tumor BRD4 depletion, antitumor efficacy, and systemic toxicity. Until these experiments are performed, the proposed PROTACs should be regarded as computationally prioritized lead hypotheses rather than experimentally confirmed active degraders.

Conclusion

This study presents an AI-assisted computational workflow for the virtual design and prioritization of BRD4-targeting PROTAC candidates using DCAF15 as the recruited E3 ligase. The workflow combined protein-structure evaluation, pharmacophore-based screening, ADMET prediction, binary docking, interaction analysis, PROTAC assembly, BRD4-DCAF15 docking, ternary-complex docking, and molecular dynamics simulation. These analyses identified a computationally prioritized CLTTMPBA-linker-E7820 PROTAC architecture with favorable predicted binding behavior and simulated ternary-complex stability.

However, the present study does not experimentally confirm biological activity. The proposed candidates have not yet been validated for cellular uptake, BRD4 target engagement, DCAF15-dependent ternary-complex formation, ubiquitination, proteasome-dependent BRD4 degradation, pancreatic cancer cell inhibition, pharmacokinetic behavior, toxicity, or in vivo antitumor efficacy. Therefore, the findings should be interpreted as computational and hypothesis-generating. Functional verification using biochemical assays, pancreatic cancer cell-based degradation assays, proteasome-rescue experiments, transcriptomic/proteomic analysis, and in vivo pancreatic cancer models is required before therapeutic activity or clinical relevance can be concluded.

Acknowledgements

This study was supported by the Medical Science Research Project of Hebei (20220104).

Disclosure of conflict of interest

None.

Address correspondence to: Filippiadis Dimitrios Konstantinos, Evgenidion University Hospital, Athens 11528, Greece. E-mail: dimitrios77k@hotmail.com; Shuo Yu, Department of Surgical Oncology, The Second Hospital of Hebei Medical University, Shijiazhuang 050000, Hebei, China. E-mail: yushuo53342022@163.com; Shaofan Qiu, Department of Gastrointestinal Surgery, The Second Hospital of Hebei Medical University, Shijiazhuang 050000, Hebei, China. E-mail: 28602153@hebmu.edu.cn

References

[1] Luo W, Wang J, Chen H, Ye L, Qiu J, Liu Y, Wang R, Weng G, Liu T, Su D, Tao J, Ding C, You L and Zhang T. Epidemiology of pancreatic cancer: new version, new vision. Chin J Cancer Res 2023; 35: 438-450.

[2] Qadir RMAB, Umair MB, Tariq UB, Ahmad A, Kiran W and Shahid MH. Unraveling pancreatic cancer: epidemiology, risk factors, and global trends. Cureus 2024; 16: e72816.

[3] Puckett Y and Garfield K. Pancreatic Cancer. 2024 Sep 10. In: StatPearls [Internet]. Treasure Island (FL): StatPearls Publishing; 2026 Jan-. PMID: 30085538.

[4] Gordon-Dseagu VL, Devesa SS, Goggins M and Stolzenberg-Solomon R. Pancreatic cancer incidence trends: evidence from the Surveillance, Epidemiology and End Results (SEER) population-based data. Int J Epidemiol 2018; 47: 427-439.

[5] Yang J, Wen C, Guo H, Chai Y, Sun G and Cheng H. Targeting early diagnosis and treatment of pancreatic cancer among the diabetic population: a comprehensive review of biomarker

screening strategies. Diabetol Metab Syndr 2025; 17: 176.
[6] Cereda V and D'Andrea MR. Pancreatic cancer: failures and hopes-a review of new promising treatment approaches. Explor Target Antitumor Ther 2025; 6: 1002299.
[7] Li B, Zhang Q, Castaneda C and Cook S. Targeted therapies in pancreatic cancer: a new era of precision medicine. Biomedicines 2024; 12: 2175.
[8] Wood LD, Canto MI, Jaffee EM and Simeone DM. Pancreatic cancer: pathogenesis, screening, diagnosis, and treatment. Gastroenterology 2022; 163: 386-402, e1.
[9] Hoang T and Tsang ES. Advances in novel targeted therapies for pancreatic adenocarcinoma. J Gastrointest Cancer 2025; 56: 38.
[10] Reiss KA, Soares KC, Torphy RJ and Gyawali B. Treatment innovations in pancreatic cancer: putting patient priorities first. Am Soc Clin Oncol Educ Book 2025; 45: e473204.
[11] Ruff SM and Pawlik TM. Molecular classification and pathogenesis of pancreatic adenocarcinoma and targeted therapies: a review. Front Biosci (Landmark Ed) 2024; 29: 101.
[12] Liu Q, Liu J, Wang S, Bao N, Zhao X and Wang L. Roles of nucleotide metabolism in pancreatic cancer. Front Immunol 2025; 16: 1637768.
[13] Devaiah BN, Gegonne A and Singer DS. Bromodomain 4: a cellular Swiss army knife. J Leukoc Biol 2016; 100: 679-686.
[14] Wang ZQ, Zhang ZC, Wu YY, Pi YN, Lou SH, Liu TB, Lou G and Yang C. Bromodomain and extraterminal (BET) proteins: biological functions, diseases and targeted therapy. Signal Transduct Target Ther 2023; 8: 420.
[15] Sun SY. Essential roles of BRD4 in cancer: DNA damage, transcription regulation, and signal transduction. Glob Transl Med 2023; 2: 3.
[16] Jin W, Tan H, Wu J, He G and Liu B. Dual-target inhibitors of bromodomain-containing protein 4 (BRD4) in cancer therapy: current situation and future directions. Drug Discov Today 2022; 27: 246-256.
[17] Sincere NI, Anand K, Ashique S, Yang J and You C. PROTACs: emerging targeted protein degradation approaches for advanced druggable strategies. Molecules 2023; 28: 4014.
[18] Zhong G, Chang X, Xie W and Zhou X. Targeted protein degradation: advances in drug discovery and clinical practice. Signal Transduct Target Ther 2024; 9: 308.
[19] He X, Weng Z and Zou Y. Progress in the controllability technology of PROTAC. Eur J Med Chem 2024; 265: 116096.
[20] Zhou Q, Wang W and Deng C. Advancements in proteolysis targeting chimeras for targeted therapeutic strategies in Alzheimer's disease. Mol Neurobiol 2025; 62: 9686-9709.
[21] Kumar H and Sobhia ME. Interplay of PROTAC complex dynamics for undruggable targets: insights into ternary complex behavior and linker design. ACS Med Chem Lett 2024; 15: 1306-1318.
[22] Abbas A and Ye F. Computational methods and key considerations for in silico design of proteolysis targeting chimera (PROTACs). Int J Biol Macromol 2024; 277: 134293.
[23] Cai H, Yao G, Shi Y, Zhang T and Hu Y. PROTAC-PatentDB: a PROTAC patent compound dataset. Sci Data 2025; 12: 1840.
[24] Shilliday F, Lucas SCC, Richter M, Michaelides IN and Fusani L. Structure of the human DDB1-DDA1-DCAF15 E3 ubiquitin ligase bound to compound furan 12. RCSB Protein Data Bank; 2024. PDB ID: 8ROX. doi:10.2210/pdb8ROX/pdb.
[25] Bai N, Miller SA, Andrianov GV, Yates M, Kirubakaran P and Karanicolas J. Rationalizing PROTAC-mediated ternary complex formation using Rosetta. J Chem Inf Model 2021; 61: 1368-1382.
[26] Ma X, Liu S, Dong X, Li X, Wang F, Zhang J, Xu Z, Shi W, Zheng A, Zhang A, Feng X and Xu L. Synthesis and evaluation of AS1411-lenalidomide-targeted degradation chimera in antitumor therapy. Pharmaceuticals (Basel) 2025; 18: 1867.
[27] Berman HM and Burley SK. Protein Data Bank (PDB): fifty-three years young and having a transformative impact on science and society. Q Rev Biophys 2025; 58: e9.
[28] Gasteiger E, Hoogland C, Gattiker A, Duvaud S, Wilkins MR, Appel RD and Bairoch A. Protein identification and analysis tools on the ExPASy server. In: Walker JM, editor. The Proteomics Protocols Handbook. Totowa, NJ: Humana Press; 2005. p. 571-607.
[29] Debnath A, Sengupta A, Rudrapal S, Kumar A and Rani M. In-silico study of molecular adaptations in halophilic Cas9. Lett Appl Microbiol 2025; 78: ovaf006.
[30] Buchan DWA, Moffat L, Lau A, Kandathil SM and Jones DT. Deep learning for the PSIPRED protein analysis workbench. Nucleic Acids Res 2024; 52: W287-W293.
[31] Jones DT. Protein secondary structure prediction based on position-specific scoring matrices. J Mol Biol 1999; 292: 195-202.
[32] Mall R, Kaushik R, Martinez ZA, Thomson MW and Castiglione F. Benchmarking protein language models for protein crystallization. Sci Rep 2025; 15: 2381.
[33] Singh H and Agrawal DK. Recent advancements in the discovery of cereblon-based protease-targeted chimeras with potential for therapeutic intervention. Future Med Chem 2022; 14: 1403-1416.

[34] Abramson J, Adler J, Dunger J, Evans R, Green T, Pritzel A, Ronneberger O, Willmore L, Ballard AJ, Bambrick J, Bodenstein SW, Evans DA, Hung CC, O'Neill M, Reiman D, Tunyasuvunakool K, Wu Z, Žemgulytė A, Arvaniti E, Beattie C, Bertolli O, Bridgland A, Cherepanov A, Congreve M, Cowen-Rivers AI, Cowie A, Figurnov M, Fuchs FB, Gladman H, Jain R, Khan YA, Low CMR, Perlin K, Potapenko A, Savy P, Singh S, Stecula A, Thillaisundaram A, Tong C, Yakneen S, Zhong ED, Zielinski M, Žídek A, Bapst V, Kohli P, Jaderberg M, Hassabis D and Jumper JM. Accurate structure prediction of biomolecular interactions with AlphaFold 3. Nature 2024; 630: 493-500.

[35] Ody BK, Zhang J, Nelson SE, Xie Y, Liu R, Dodd CJ, Jacobs SE, Whitzel SL, Williams LA, Gozem S, Turlington M and Yin J. Synthesis and evaluation of cereblon-recruiting HaloPROTACs. Chembiochem 2023; 24: e202300498.

[36] Pilotto A, Carini M, Bresciani R, Monti E, Ferrari F, De Francesco MA, Padovani A and Biasiotto G. Next generation sequencing analysis in patients affected by Parkinson's disease and correlation between genotype and phenotype in selected clinical cases. Int J Mol Sci 2025; 26: 2397.

[37] Polák L, Škoda P, Riedlová K, Krivák R, Novotný M and Hoksza D. PrankWeb 4: a modular web server for protein-ligand binding site prediction and downstream analysis. Nucleic Acids Res 2025; 53: W466-W471.

[38] Jendele L, Krivak R, Skoda P, Novotny M and Hoksza D. PrankWeb: a web server for ligand binding site prediction and visualization. Nucleic Acids Res 2019; 47: W345-W349.

[39] Dong J and Hao X. Pharmacophore screening, molecular docking, and MD simulations for identification of VEGFR-2 and c-Met potential dual inhibitors. Front Pharmacol 2025; 16: 1534707.

[40] Hsia O, Hinterndorfer M, Cowan AD, Iso K, Ishida T, Sundaramoorthy R, Nakasone MA, Imrichova H, Schätz C, Rukavina A, Husnjak K, Wegner M, Correa-Sáez A, Craigon C, Casement R, Maniaci C, Testa A, Kaulich M, Dikic I, Winter GE and Ciulli A. Targeted protein degradation via intramolecular bivalent glues. Nature 2024; 627: 204-211.

[41] Momin Y, Beloshe V. Pharmacophore modeling in drug design. In: Narayan CV, Verma S, Grewal AS, Singh N and Nimesh H. Revolutionizing drug discovery: cutting-edge computational techniques. Advances in Pharmacology, Cambridge: Academic Press; 2025. pp. 313-324.

[42] Kim S, Chen J, Cheng T, Gindulyte A, He J, He S, Li Q, Shoemaker BA, Thiessen PA, Yu B, Zaslavsky L, Zhang J and Bolton EE. PubChem 2025 update. Nucleic Acids Res 2025; 53: D1516-D1525.

[43] Huang Z, Zhao J, Yang L, Zhu J and Zhang R. MView: a pre- and post-processing tool for quantum chemistry calculation. J Chem Phys 2025; 162: 132501.

[44] Wu R, Zhang T, Zhao S, Maccarana M, Li JP, Li C and Cao H. Design, synthesis, and anti-inflammatory potential of PROTAC drug molecules based on fondaparinux sodium. Front Bioeng Biotechnol 2025; 13: 1597344.

[45] Ge J, Li S, Weng G, Wang H, Fang M, Sun H, Deng Y, Hsieh CY, Li D and Hou T. PROTAC-DB 3.0: an updated database of PROTACs with extended pharmacokinetic parameters. Nucleic Acids Res 2025; 53: D1510-D1515.

[46] Afrdi MB, Sardar H, Serdaroğlu G, Shah SWA, Alsharif KF and Khan H. In silico ADMET and DFT analysis of methoxy substituted curcumin derivatives. Inorg Chem Commun 2024; 168: 112943.

[47] Fu L, Shi S, Yi J, Wang N, He Y, Wu Z, Peng J, Deng Y, Wang W, Wu C, Lyu A, Zeng X, Zhao W, Hou T and Cao D. ADMETlab 3.0: an updated comprehensive online ADMET prediction platform enhanced with broader coverage, improved performance, API functionality and decision support. Nucleic Acids Res 2024; 52: W422-W431.

[48] Thakur H and Das A. Comparative analysis of in silico tools for drug side effect prediction. In: 2025 International Conference on Intelligent Control, Computing and Communications. Piscataway: IEEE; 2025. pp. 295-298.

[49] Liu Y, Yang X, Gan J, Chen S, Xiao ZX and Cao Y. CB-Dock2: improved protein-ligand blind docking by integrating cavity detection, docking and homologous template fitting. Nucleic Acids Res 2022; 50: W159-W164.

[50] Kochnev Y, Ahmed M, Maldonado AM and Durrant JD. MolModa: accessible and secure molecular docking in a web browser. Nucleic Acids Res 2024; 52: W498-W506.

[51] Agu PC, Afiukwa CA, Orji OU, Ezeh EM, Ofoke IH, Ogbu CO, Ugwuja EI and Aja PM. Molecular docking as a tool for the discovery of molecular targets of nutraceuticals in diseases management. Sci Rep 2023; 13: 13398.

[52] Bultum LE, Tolossa GB, Kim G, Kwon O and Lee D. In silico activity and ADMET profiling of phytochemicals from Ethiopian indigenous aloes using pharmacophore models. Sci Rep 2022; 12: 22221.

[53] PerkinElmer, Inc. PerkinElmer Brings ChemDraw Software to the Cloud, Enhancing Search and Collaboration Workflows. Business Wire. November 10, 2020.

[54] Rajendran P, Rathinasabapathy R, Chandra Kishore S and Bellucci S. Computational-simu-

lation-based behavioral analysis of chemical compounds. J Compos Sci 2023; 7: 196.
[55] Hasan MB, Rahman MJ, Das R, Akter T, Hosen MS, Kona UMP and Uzzaman M. Physicochemical, biological, and toxicological studies of pyridine and its derivatives: an in-silico approach. Discover Chemistry 2025; 2: 70.
[56] Veg E, Hashmi K, Satya, Joshi S and Khan T. Computational drug-likeness studies of selected thiosemicarbazones: a sustainable approach for drug designing. MDPI Proceedings 2025; 87: 35.
[57] Rustagi V, Gupta SRR, Singh A and Singh IK. Beyond trial and error: leveraging advanced software for therapeutic discovery. Chem Biol Lett 2025; 12: 1.
[58] Sankaranarayanan P, Dicky John Davis G, Pa A, Manikandan M and Ghosh A. Molecular docking and MD simulation approach to identify potential phytochemical lead molecule against triple negative breast cancer. F1000Res 2025; 13: 1271.
[59] Shaik S, Kumar Reddy Gayam P, Chaudhary M, Singh G and Pai A. Advances in designing ternary complexes: integrating in-silico and biochemical methods for PROTAC optimisation in target protein degradation. Bioorg Chem 2024; 153: 107868.
[60] Burslem GM and Crews CM. Proteolysis-targeting chimeras as therapeutics and tools for biological discovery. Cell 2020; 181: 102-114.
[61] Zengerle M, Chan KH and Ciulli A. Selective small molecule induced degradation of the BET bromodomain protein BRD4. ACS Chem Biol 2015; 10: 1770-1777.
[62] Zhang X, Song Z, Zhang X, Zou J, Yu G, Chen X and Wang S. Unconventional PROTACs for targeted protein degradation in cancer therapy. Angew Chem Int Ed Engl 2025; 64: e202507702.
[63] Kanbar K, El Darzi R and Jaalouk DE. Precision oncology revolution: CRISPR-Cas9 and PROTAC technologies unleashed. Front Genet 2024; 15: 1434002.
[64] Chou CL, Lin CT, Kao CT and Lin CC. A novel rational PROTACs design and validation via AI-driven drug design approach. ACS Omega 2024; 9: 38371-38384.
[65] Pan Y, Wang Y and Gou S. Proteolysis targeting chimera, molecular glue degrader and hydrophobic tag tethering degrader for targeted protein degradation: mechanisms, strategies and application. Bioorg Chem 2025; 161: 108491.
[66] Wu KY, Hung TI and Chang CA. PROTAC-induced protein structural dynamics in targeted protein degradation. Elife 2025; 13: RP101127.
[67] Li YQ, Lannigan WG, Davoodi S, Daryaee F, Corrionero A, Alfonso P, Rodriguez-Santamaria JA, Wang N, Haley JD and Tonge PJ. Discovery of novel Bruton's tyrosine kinase PROTACs with enhanced selectivity and cellular efficacy. J Med Chem 2023; 66: 7454-7474.
[68] Winter GE, Buckley DL, Paulk J, Roberts JM, Souza A, Dhe-Paganon S and Bradner JE. Phthalimide conjugation as a strategy for in vivo target protein degradation. Science 2015; 348: 1376-1381.
[69] Luo H, Tian Y, Abdullah R, Zhang B, Ma Y and Zhang G. Advancing design strategy of PROTACs for cancer therapy. MedComm 2025; 6: e70258.
[70] Raina K, Lu J, Qian Y, Altieri M, Gordon D, Rossi AM, Wang J, Chen X, Dong H, Siu K, Winkler JD, Crew AP, Crews CM and Coleman KG. PROTAC-induced BET protein degradation as a therapy for castration-resistant prostate cancer. Proc Natl Acad Sci U S A 2016; 113: 7124-7129.
[71] Gadd MS, Testa A, Lucas X, Chan KH, Chen W, Lamont DJ, Zengerle M and Ciulli A. Structural basis of PROTAC cooperative recognition for selective protein degradation. Nat Chem Biol 2017; 13: 514-521.
[72] Juan A, Noblejas-López MDM, Arenas-Moreira M, Alonso-Moreno C and Ocaña A. Options to improve the action of PROTACs in cancer: development of controlled delivery nanoparticles. Front Cell Dev Biol 2022; 9: 805336.
[73] Drummond ML and Williams CI. In silico modeling of PROTAC-mediated ternary complexes: validation and application. J Chem Inf Model 2019; 59: 1634-1644.

Supplementary Table 1. Multi-parameter validation and comparative structural evaluation of BRD4 and DCAF15 protein models

Validation parameter	Purpose of analysis	BRD4	DCAF15 E3 ligase complex	Interpretation
PDB reference structure	Experimental/comparative template	3MXF	8ROX	Experimentally resolved structures used as reference templates
Number of residues evaluated	Structural coverage	127	1541	Full structural models were considered for validation
Ramachandran favored residues (%)	Backbone stereochemical quality	95.5	87.5	BRD4 showed excellent backbone geometry; DCAF15 showed acceptable backbone quality for a large multidomain complex
Ramachandran allowed residues (%)	Additional acceptable conformational space	4.5	11.7	Most remaining residues were located in allowed conformational regions
Ramachandran outliers (%)	Disallowed backbone conformations	0.0	0.8	Very low outlier percentage indicates no major stereochemical abnormality
Mean pLDDT score	AlphaFold local model confidence	91.8	82.6	BRD4 showed very high local confidence; DCAF15 showed good confidence with expected lower confidence in flexible loop/domain regions
Mean PAE value (Å)	Relative domain-orientation reliability	2.1	5.4	Low PAE for BRD4 indicates reliable local/global orientation; moderate PAE for DCAF15 reflects multidomain flexibility
MolProbity score	Overall all-atom model quality	1.42	1.98	Lower values indicate acceptable all-atom geometry and model quality
Clashscore	Steric-overlap assessment	3.8	8.6	Low clashscores indicate limited unfavorable atomic contacts
Poor rotamers (%)	Side-chain conformational quality	1.2	3.7	Low percentage of poor rotamers supports acceptable side-chain packing
Cβ deviations	Local geometry abnormality	0	4	Minimal Cβ deviations indicate absence of major local geometric distortions
ERRAT quality factor (%)	Non-bonded interaction quality	94.1	86.9	Scores above acceptable limits indicate reliable non-bonded atomic interactions
Verify 3D pass residues (%)	Compatibility between sequence and 3D environment	93.7	84.7	Most residues showed compatible 1D-3D structural environments
ProSA Z-score	Global energetic plausibility	-5.62	-14.36	Z-scores fall within the expected range for native-like protein structures of comparable size
QMEAN Z-score	Composite global model-quality estimate	-0.92	-1.68	Values close to zero or moderately negative support acceptable model quality
RMSD versus reference PDB structure (Å)	Structural similarity after superposition	0.76	1.89	Low RMSD values indicate strong agreement with experimental reference structures
TM-score versus reference PDB structure	Fold-level structural similarity	0.93	0.86	TM-scores above 0.80 indicate preservation of the experimentally observed fold
Binding-pocket confidence	Reliability of docking-relevant regions	High	Moderate to high	Predicted binding regions were located mainly in structurally reliable regions
Overall validation status	Final structural suitability	Highly reliable	Acceptable/reliable	Both structures were considered suitable for downstream docking, PROTAC modeling, and MD simulation

Supplementary Table 2. Comparative summary of docking and post-docking analyses used for BRD4-DCAF15 PROTAC prioritization

Tool/software	Analysis level	Molecular system/input	Main output metric	Key result obtained	Selection/interpretation criterion	Role in final prioritization
PRANK-WEB	Binding-pocket prediction	Prepared BRD4 and DCAF15 structures	Pocket score, probability, number of pocket residues	BRD4 showed two predicted ligand-binding pockets; DCAF15 showed multiple predicted ligandable sites, with the top-ranked DCAF15 pocket showing the highest score and residue coverage	Highest-ranked pockets were considered more reliable for docking interpretation	Defined plausible ligand-binding regions before docking
Pharmit	Pharmacophore-based virtual screening	BRD4-JQ1 pharmacophore model screened against PubChem 3D conformer library	Pharmacophore fit, shape complementarity, RMSD	Ten BRD4 ligand candidates were shortlisted from PubChem hits	Hits with essential pharmacophore-feature matching and low RMSD were retained	Generated the initial BRD4 ligand library for ADMET and docking
ADMETlab 3.0	Developability filtering	Shortlisted BRD4 ligand candidates	ADMET acceptability and Lipinski compliance	MCTTB, CLTTMPBA, and CTTMPBA showed acceptable ADMET and Lipinski profiles; CTIP showed partial acceptability despite strong docking affinity	Ligands were not selected by docking score alone; ADMET/Lipinski behavior was integrated with binding affinity	Helped avoid prioritization of ligands with poor predicted pharmacokinetic or drug-likeness behavior
CB-Dock2	Binary protein-ligand docking	BRD4 with pharmacophore-screened ligands	Predicted binding affinity and docking pose	CTIP showed the strongest predicted binding affinity of -10.4 kcal/mol, followed by CLTTMPBA and CTA at -9.7 kcal/mol; MCTTB and CTTA2MP showed -9.1 and -8.9 kcal/mol, respectively	More negative docking energy and proper localization in the predicted BRD4 pocket indicated stronger predicted binding	Identified high-affinity BRD4-binding scaffolds; CLTTMPBA was selected because it balanced strong docking affinity with acceptable ADMET/Lipinski behavior
CB-Dock2	Binary protein-ligand docking	DCAF15 with E7820	Predicted binding affinity and docking pose	E7820 was docked into the DCAF15 ligand-binding region; binding affinity	Binding pose was evaluated based on pocket localization, absence of severe steric clashes, and stabilizing residue-level contacts	Supported E7820 as the DCAF15-recruiting moiety for PROTAC construction
Discovery Studio Visualizer	Post-docking interaction analysis	BRD4-CLTTMPBA docked complex	Hydrogen bonds, carbon-hydrogen bonds, π-π stacking, π-alkyl contacts, alkyl contacts, sulfur-mediated contacts, and interaction distances	CLTTMPBA showed stabilizing interactions with residues including TYR78, CYS84, ASP87, PHE42, PHE88, MET91, PHE92, LEU30, LEU33, ILE69, and PHE116	Interaction quality, residue involvement, and contact distance were used to confirm whether docking affinity reflected meaningful binding contacts	Confirmed that CLTTMPBA was not prioritized only by docking score but also by favorable residue-level interaction quality
Discovery Studio Visualizer	Post-docking interaction analysis	DCAF15-E7820 docked complex	Hydrogen bonds and aromatic interactions	E7820 showed key interactions involving TRP600 and TYR598, including hydrogen bonding and multiple π-π stacked interactions with distances of approximately 2.65-4.89 Å	Stable polar and aromatic interactions supported recognition of the DCAF15-recruiting ligand	Supported the suitability of E7820 for recruiting DCAF15 in the proposed PROTAC architecture

HADDOCK	Protein-protein docking	BRD4 with DDB1-DDA1-DCAF15 complex	HADDOCK score, cluster population, fraction of common contacts, interface RMSD, van der Waals energy, electrostatic energy, and desolvation energy	Cluster 2 showed the most favorable overall docking behavior, with an average HADDOCK score of approximately -85, favorable fraction of common contacts, and low interface-RMSD distribution	The best cluster was selected using both energetic favorability and pose convergence, not only the lowest single docking score	Provided the BRD4-DCAF15 spatial arrangement used for subsequent PROTAC-mediated ternary-complex docking
PyRx/ AutoDock Vina	PROTAC-mediated ternary-complex docking	BRD4-DCAF15 receptor complex with assembled CLTTMPBA-linker-E7820 PROTAC	Vina binding affinity, docking pose, linker orientation, steric compatibility, and simultaneous receptor engagement	The optimized PROTAC was docked into the selected BRD4-DCAF15 model; final Vina score	The final pose was selected based on simultaneous engagement of BRD4 and DCAF15 binding regions, absence of severe steric clashes, and favorable linker orientation	Evaluated whether the assembled PROTAC could geometrically bridge BRD4 and DCAF15 in the predicted ternary complex
Discovery Studio Visualizer	Ternary-complex interaction analysis	BRD4-PROTAC-DCAF15 docked complex	Protein-PROTAC contacts at both BRD4 and DCAF15 interfaces	The selected ternary-complex pose retained stabilizing contacts at both protein-binding ends of the PROTAC	Dual-interface interaction quality was used to assess whether the PROTAC could maintain simultaneous engagement of the target protein and E3 ligase	Supported the structural feasibility of the proposed ternary-complex model
Schrödinger MD	Post-docking dynamic stability assessment	BRD4-PROTAC-DCAF15 ternary complex	RMSD, RMSF, hydrogen-bond persistence, SASA, radius of gyration, contact occupancy, and interaction-energy components	The 500 ns MD simulation was used to determine whether the docked ternary complex remained stable after dynamic relaxation	Stable RMSD plateau, limited interface RMSF, persistent contacts, and stable compactness parameters supported dynamic stability	Provided post-docking support for ternary-complex stability, but not experimental proof of BRD4 degradation